Inorganic Chemistry
Article

Inorg. Chem. **2010**, *49*, 6409–6420 **6409**
DOI: 10.1021/ic100484a

Secondary Coordination Sphere Interactions within the Biomimetic Iron Azadithiolate Complexes Related to Fe-Only Hydrogenase: Dynamic Measure of Electron Density about the Fe Sites

Yu-Chiao Liu,[†] Ling-Kuang Tu,[†] Tao-Hung Yen,[†] Gene-Hsiang Lee,[‡] Shu-Ting Yang,[†] and Ming-Hsi Chiang*,[†]

[†] *Institute of Chemistry, Academia Sinica, Nankang, Taipei 115, Taiwan, and* [‡] *Instrumentation Center, National Taiwan University, Taipei 106, Taiwan*

Received December 23, 2009

A series of iron azadithiolate complexes possessing an intramolecular secondary coordination sphere interaction and an ability to reduce HOAc at the potential near the first electron-transfer process are reported. A unique structural feature in which the aza nitrogen has its lone pair point toward the apical carbonyl carbon is observed in $[Fe_2(\mu\text{-}S(CH_2)_2NR(CH_2)_2S)(CO)_{6-x}L_x]_2$ (R = ^{n}Pr, x = 0, **1a**; R = ^{i}Pr, x = 0, **1b**; R = ^{n}Pr, L = PPh_3, x = 1, **2**; R = ^{n}Pr, L = P^nBu_3, x = 1, **3**) as biomimetic models of the active site of Fe-only hydrogenase. The presence of this weak $N\cdots C(CO_{ap})$ interaction provides electronic perturbation at the Fe center. The distance of the $N\cdots C(CO_{ap})$ contact is 3.497 Å in **1a**. It increases by 0.455 Å in **2** when electronic density of the Fe site is slightly enriched by a weak σ-donating ligand, PPh_3. A longer distance (4.040 Å) is observed for the P^nBu_3 derivative, **3**. This $N\cdots C(CO_{ap})$ distance is thus a dynamic measure of electronic nature of the Fe_2 core. Variation of electronic richness within the Fe_2 moiety among the complexes reflects on their electrochemical response. Reduction of **2** is recorded at the potential of −2.17 V, which is 270 mV more negative than that of **1**. Complex **3** requires additional 150 mV for the same reduction. Such cathodic shift results from CO substitution by phosphines. Electrocatalytic hydrogen production from HOAc by both kinds of complexes (all-CO and phosphine-substituted species) requires the potential close to that for reduction of the parent molecules in the absence of acids. The catalytic mechanism of **1a** is proposed to involve proton uptake at the Fe^0Fe^I redox level instead of the Fe^0Fe^0 level. This result is the first observation among the all-CO complexes with respect to electrocatalysis of HOAc.

Introduction

In recent years, high efficiency ($6 \times 10^3\ s^{-1}$) of Fe-only hydrogenase in H_2 production at a mild reduction potential (−0.1 to −0.5 V) has stimulated great interests of synthetic chemists in modeling its active site to understand the electrocatalytic mechanism of hydrogen evolution and eventually develop a cheap substitute for platinum electrodes.[1] Chemists have taken advantages of organometallic complexes $[Fe_2(\mu\text{-}SR)_2(CO)_6]$ for the pursuit of their structural resemblance to the active site of Fe-only hydrogenase.[2] To achieve higher turnover rates and lower working reduction potentials, a two-faceted strategy is employed in recent studies: introduction of the basic site to assist proton delivery to the catalytic Fe center and ligand substitution to enrich electron density of the Fe_2 subunit.

It has been shown from the experimental results that a secondary amine N is a preferred candidate for the bridgehead of the dithiolate linker.[3] Hydrogen production catalyzed by $[Fe_2(\mu\text{-adt})(CO)_6]$ (adt = SCH_2NRCH_2S) requires the reduction potential about 250 mV less compared to its pdt analogue $[Fe_2(\mu\text{-pdt})(CO)_6]$ (pdt = $S(CH_2)_3S$).[4] The aza nitrogen site being a moderate base facilitates *N*-protonation in contact of stronger acids, which will further diminish the reduction potential by about 400 mV.[5,6] Recent results by Rauchfuss et al. have shown that the catalytic rate is enhanced in the presence of the amine nitrogen site.[7] In addition, a density functional theory (DFT) calculation indicates that

---

*To whom correspondence should be addressed. E-mail: mhchiang@chem.sinica.edu.tw.

(1) (a) Cammack, R.; Frey, M.; Robson, R. *Hydrogen as a Fuel: Learning from Nature*; Taylor & Francis: London and New York, 2001. (b) Tard, C.; Pickett, C. J. *Chem. Rev.* **2009**, *109*, 2245–2274. (c) Gloaguen, F.; Rauchfuss, T. B. *Chem. Soc. Rev.* **2009**, *38*, 100–108.

(2) (a) Seyferth, D.; Henderson, R. S.; Song, L. C. *Organometallics* **1982**, *1*, 125–133. (b) Dahl, L. F.; Wei, C.-H. *Inorg. Chem.* **1963**, *2*, 328–333.

(3) Silakov, A.; Wenk, B.; Reijerse, E.; Lubitz, W. *Phys. Chem. Chem. Phys.* **2009**, *11*, 6592–6599.

(4) (a) Ott, S.; Kritikos, M.; Åkermark, B.; Sun, L.; Lomoth, R. *Angew. Chem., Int. Ed.* **2004**, *43*, 1006–1009. (b) Capon, J.-F.; Ezzaher, S.; Gloaguen, F.; Pétillon, F. Y.; Schollhammer, P.; Talarmin, J.; Davin, T. J.; McGrady, J. E.; Muir, K. W. *New J. Chem.* **2007**, *31*, 2052–2064.

(5) Chiang, M.-H.; Liu, Y.-C.; Yang, S.-T.; Lee, G.-H. *Inorg. Chem.* **2009**, *48*, 7604–7612.

(6) (a) Ezzaher, S.; Orain, P.-Y.; Capon, J.-F.; Gloaguen, F.; Pétillon, F. Y.; Roisnel, T.; Schollhammer, P.; Talarmin, J. *Chem. Commun.* **2008**, 2547–2549. (b) Wang, N.; Wang, M.; Zhang, T.; Li, P.; Liu, J.; Sun, L. *Chem. Commun.* **2008**, 5800–5802. (c) Ezzaher, S.; Capon, J.-F.; Gloaguen, F.; Pétillon, F. Y.; Schollhammer, P.; Talarmin, J.; Kervarec, N. *Inorg. Chem.* **2009**, *48*, 2–4.

the aza nitrogen bridgehead can stabilize the inverted geometry of the $\{Fe(CO)_3\}$ moiety in $[Fe_2(\mu\text{-adt})(CO)_6]$ by donating electron density to the vacant site of the Fe center.[8] These experimental and theoretical results suggest that the aza nitrogen atom in the dithiolate bridge plays a key role in the enzymatic production of hydrogen.

Proton insertion to the Fe−Fe vector can not occur in $[Fe_2(\mu\text{-SS})_2(CO)_6]$ (SS = dithiolate bridges) unless the electron density about the Fe centers is significantly increased by ligation of stronger donating ligands resulted from the CO substitution.[9,10] The result may answer why the active site of Fe-only hydrogenase consists of cyanides in the primary ligation site. Unfortunately, substitution with stronger σ-donating ligands causes the undesired effect on working potentials of the unprotonated species.[11] When CO in $[Fe_2(\mu\text{-SS})_2(CO)_6]$ is replaced by phosphines, the reduction potential shifts toward a more negative region by about 300−700 mV.[5] The same trend applies for CN^- and isocyanide by 600 and 200 mV, respectively.[12] To overcome this kind of negative impact, mother nature might have discovered her own solutions where the CN^- groups in the active site of Fe-only hydrogenase are hydrogen bonded to regulate the electron density flux into the catalytic Fe site.[13]

As a matter of fact, the active site of Fe-only hydrogenase is encapsulated inside the protein pocket in which numerous hydrogen bonds between the CN^- ligands and the peptide backbone are present. Two amino acid residues, Lys^{358} and Ser^{232}, form hydrogen bonds with the CN^- groups of the H-cluster in *Clostridium pasteurianum* (CpI).[14] As for *Desulfovibrio desulfuricans* (DdH), Lys^{237} and the peptide-chain nitrogen atoms of Ala^{109} and Ile^{204} are in close contacts with the cyanides.[15] In addition to the structural purpose, these weak intermolecular interactions serve the functional role to modulate electronic structure of the Fe centers, that is, the redox potentials of the active site. Effects of interactions in the secondary coordination sphere on reduction potentials have been observed in several classes of metalloproteins such as iron−sulfur proteins (ferredoxins, Fds and high-potential iron proteins, HiPIPs)[16] and cupredoxins.[17]

If interactions of the secondary coordination sphere are to regulate the electronic structure of the Fe centers, it might be able to monitor electronic richness about the Fe sites by the interaction. Herein, we report examples based on this concept. The intramolecular interaction between the aza nitrogen and the apical carbonyl carbon within $[Fe_2(\mu\text{-}S(CH_2)_2NR(CH_2)_2S)(CO)_{6-x}L_x]_2$ changes with phosphine substitution of the Fe_2 moiety, which suggests the interaction is a dynamic measure of electron density about the Fe centers. The electrocatalytic property of these complexes in the presence of HOAc is discussed.

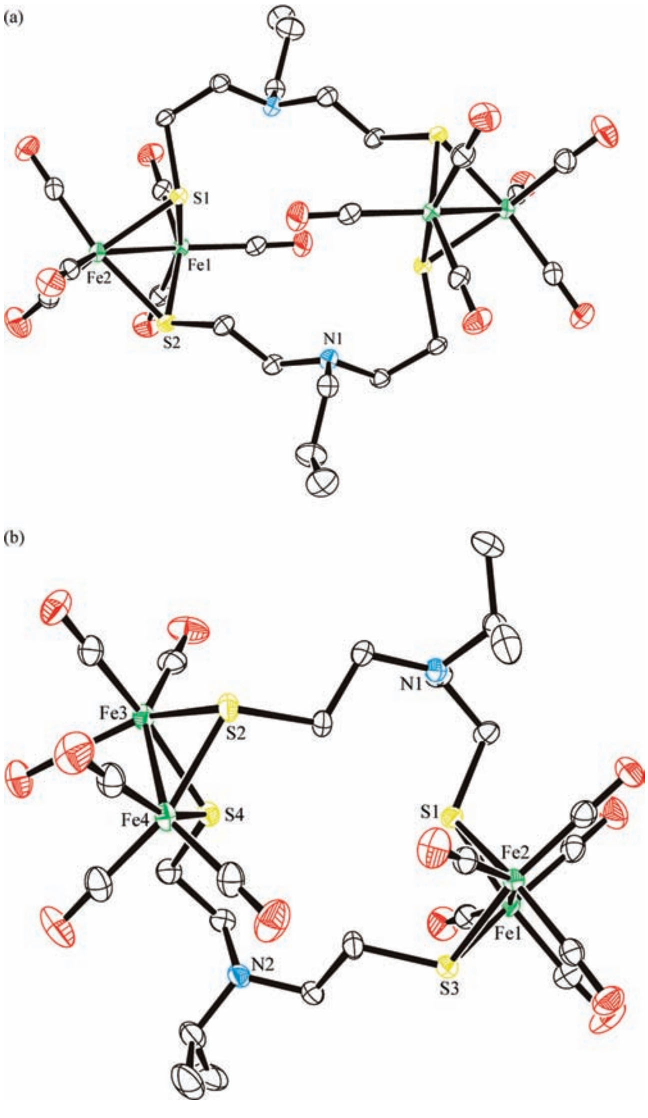

Figure 1. Molecular structures of $[Fe_2(\mu\text{-}S(CH_2)_2NR(CH_2)_2S)(CO)_6]_2$, ((a) R = ^{n}Pr, **1a**; (b) R = ^{i}Pr, **1b**), thermal ellipsoids drawn at 50% probability level. All hydrogen atoms are omitted for clarity. Selected bond lengths (Å) and angles (deg) for **1a**: Fe−Fe, 2.5234(4); Fe−S, 2.2565; Fe−$C_{CO,ap}$, 1.807; Fe−$C_{CO,ba}$, 1.791; S−Fe−S, 81.058; S−Fe−Fe, 56.005; Fe−S−Fe, 67.991; for **1b**: Fe−Fe, 2.503; Fe−S, 2.259; Fe−$C_{CO,ap}$, 1.803; Fe−$C_{CO,ba}$, 1.788; S−Fe−S, 81.27; S−Fe−Fe, 56.365; Fe−S−Fe, 67.27.

Results and Discussion

$[Fe_2(\mu\text{-}S(CH_2)_2NR(CH_2)_2S)(CO)_6]_2$ (R = ^{n}Pr, **1a**; ^{i}Pr, **1b**) were synthesized based on the procedures previously described.[5] Complexes **1a** and **1b** both crystallize in $P2_1/c$ space group. Crystals of the same complex, $\mathbf{1a_{asym}}$, with lower symmetry characterized in the $P2_1/n$ space group were also grown from the same solvent system. Their metric data and molecular structure are given in Figure 1 and Supporting Information, Figure *S1*. The average Fe−Fe bond lengths of

---

(7) Barton, B. E.; Olsen, M. T.; Rauchfuss, T. B. *J. Am. Chem. Soc.* **2008**, *130*, 16834–16835.

(8) Tye, J. W.; Darensbourg, M. Y.; Hall, M. B. *Inorg. Chem.* **2006**, *45*, 1552–1559.

(9) Zhao, X.; Georgakaki, I. P.; Miller, M. L.; Yarbrough, J. C.; Darensbourg, M. Y. *J. Am. Chem. Soc.* **2001**, *123*, 9710–9711.

(10) Gloaguen, F.; Lawrence, J. D.; Rauchfuss, T. B. *J. Am. Chem. Soc.* **2001**, *123*, 9476–9477.

(11) (a) Tye, J. W.; Lee, J.; Wang, H.-W.; Mejia-Rodriguez, R.; Reibenspies, J. H.; Hall, M. B.; Darensbourg, M. Y. *Inorg. Chem.* **2005**, *44*, 5550–5552. (b) Morvan, D.; Capon, J.-F.; Gloaguen, F.; Le Goff, A.; Marchivie, M.; Michaud, F.; Schollhammer, P.; Talarmin, J.; Yaouanc, J.-J.; Pichon, R.; Kervarec, N. *Organometallics* **2007**, *26*, 2042–2052.

(12) Gloaguen, F.; Lawrence, J. D.; Schmidt, M.; Wilson, S. R.; Rauchfuss, T. B. *J. Am. Chem. Soc.* **2001**, *123*, 12518–12527.

(13) Nicolet, Y.; Lemon, B. J.; Fontecilla-Camps, J. C.; Peters, J. W. *Trends Biochem. Sci.* **2000**, *25*, 138–143.

(14) Peters, J. W.; Lanzilotta, W. N.; Lemon, B. J.; Seefeldt, L. C. *Science* **1998**, *282*, 1853–1858.

(15) Nicolet, Y.; Piras, C.; Legrand, P.; Hatchikian, C. E.; Fontecilla-Camps, J. C. *Structure* **1999**, *7*, 13–23.

(16) Low, D. W.; Hill, M. G. *J. Am. Chem. Soc.* **2000**, *122*, 11039–11040.

(17) Berry, S. M.; Ralle, M.; Low, D. W.; Blackburn, N. J.; Lu, Y. *J. Am. Chem. Soc.* **2003**, *125*, 8760–8768.

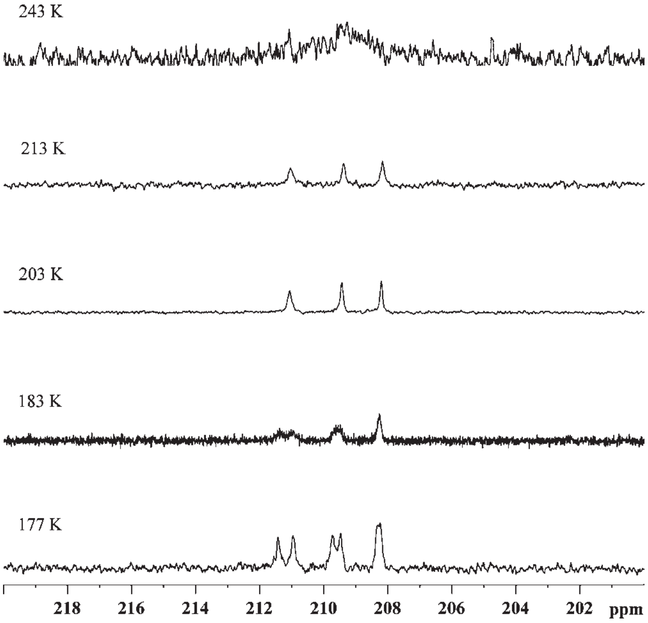

Figure 2. Low-field ^{13}C NMR of **1b** at various temperatures showing carbonyl resonances.

1a and **1b** are 2.512 and 2.503 Å, respectively, which is slightly shorter than values reported in the protein structures by 0.1 Å.[14,15] The particular structural feature of **1a** and **1b**, as shown in Figure 1 and Supporting Information, Figure *S1*, is that lone pairs from the central nitrogen atoms of the dithiolate bridges point toward the apical CO ligand on each Fe_2S_2 unit. The N···C(CO_{ap}) distances from this intramolecular interaction are measured to be 3.497 and 4.011 Å on average for **1a** and **1b**, respectively. The results infer that there is a tendency for the nitrogen atom to interact with the CO_{ap} group albeit these values are larger than the sum of van der Waals radius of carbon (1.7 Å) and nitrogen (1.55 Å).[18] The presence of such interaction is reflected on the lower energy of the ν(CO) stretching bands in the IR spectra (Supporting Information, Figure *S2*, Table *S2*). The longer N···C(CO_{ap}) distance of **1b** is realized by the steric effect of the *i*-propyl group compared with its less bulky *n*-propyl analogue. This assumption is made on the basis of the result from the only related species, $[Fe_2(\mu\text{-}S(CH_2)_2O(CH_2)_2S)(CO)_6]_2$, where a short separation of 3.182 Å, compared to van der Waals contact of O···C_{CO} of 3.22 Å, between the central oxygen atom and the CO_{ap} ligand is observed.[19] Recently, DuBois et al have reported characterization of $[Ni(L)(P^{Cy}{}_2N^{Bz}{}_2)_2](BF_4)_2$ (L = CO, CNCy) in which CO/CNR ligand is stabilized by intramolecular interactions of the second coordination sphere between the lone pairs of the nitrogen atoms on the diphosphine chelates and the partially positive carbon atom of CO or CNR.[20] If the N···C interactions are absent, isolation of $[Ni(L)(P^{Cy}{}_2N^{Bz}{}_2)_2](BF_4)_2$ and its related diphosphine-chelated derivatives is unsuccessful, so influences of the second coordination sphere interaction in the Ni^{II} complexes are not available for comparison from the ν(CO) IR band energy. In the current study, ν(CO) bands of **1a** and **1b** shift toward lower energy by at least 5 cm^{-1}.

The presence of the N···C(CO_{ap}) contact would yield the asymmetry of the molecule. Figure 2 displays a selection of the various temperature ^{13}C NMR spectra of **1b** for the CO region. One sharp resonance at 208.96 ppm is observed at 298 K. It broadens as the temperature is decreased and coalesces into the baseline at 243 K. Three sharp bands in an intensity ratio of 1: 1: 1 located at 211.07, 209.43, and 208.21 ppm are apparent at 203 K. These resonances progressively broaden again and separate into two equal intensity signals each in the course of 203−177 K. It is realized that the weak interaction between the apical CO groups and the amine units, which hinders the free rotation of the CO ligands, becomes a greater role below 203 K.

If this intramolecular interaction is mainly due to the electronic factor instead of the crystal packing, its presence tentatively suggests that the Fe_2 moiety is relatively electron deficient and that the N···C(CO_{ap}) distance can be treated as an indirect measure of the electronic nature of the Fe_2 subunit. One shall be able to vary this distance by tuning electron density about the Fe centers. To exert minimal electronic influence on the Fe site, PPh_3 being a weak σ-donating substitute is used. When two CO groups of **1a** are replaced by PPh_3, $[Fe_2(\mu\text{-}S(CH_2)_2N^nPr(CH_2)_2S)(CO)_5(PPh_3)]_2$, **2**, is prepared as the main IR band of its parent molecule shifts from 2037 cm^{-1} to lower frequency by 58 cm^{-1}. This energy change reflects on observations of electrochemistry in which the Fe-core reduction occurs at more negative potential (vide infra) and structural characterization where the N···C(CO_{ap}) contact is lengthened. Complex **2** crystallizes in the *P*1 bar space group with the PPh_3 groups occupying the apical positions of the Fe centers. Selected metric data are listed in the Figure 3 caption, and its structure is shown in Figure 3 as the thermal ellipsoid plot. It is obvious that the N···C(CO_{ap}) interaction is preserved in **2**, but the distance is lengthened by 0.455 Å to 3.952 Å. This longer distance suggests a weaker interaction with respect to **1a** owing to that PPh_3 increases electron density about the Fe core.

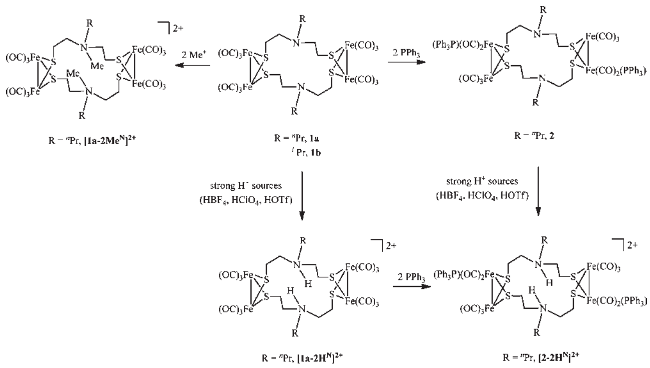

The intramolecular interaction can be removed upon methylation or protonation of the amine nitrogen atom. $[Fe_2(\mu\text{-}S(CH_2)_2N^nPr(Me)(CH_2)_2S)(CO)_6]_2{}^{2+}$, $\mathbf{[1a\text{-}2Me^N]^{2+}}$, is prepared in high yields when the parent molecule reacts with $CF_3SO_3CH_3$ (MeOTf). Identical CO vibrational patterns indicate that the structure remains intact upon methylation, which is also confirmed by structural characterization. The energy of the IR bands of the *N*-methylated product is

---

[18] (a) Batsanov, S. S. *Inorg. Mater.* **2001**, *37*, 871–885. (b) Pauling, L. *J. Am. Chem. Soc.* **1929**, *51*, 1010–1026. (c) Pauling, L. *J. Am. Chem. Soc.* **1947**, *69*, 542–553.

[19] Song, L.-C.; Gao, J.; Wang, H.-T.; Hua, Y.-J.; Fan, H.-T.; Zhang, X.-G.; Hu, Q.-M. *Organometallics* **2006**, *25*, 5724–5729.

[20] (a) Wilson, A. D.; Fraze, K.; Twamley, B.; Miller, S. M.; DuBois, D. L.; DuBois, M. R. *J. Am. Chem. Soc.* **2008**, *130*, 1061–1068. (b) DuBois, M. R.; DuBois, D. L. *Chem. Soc. Rev.* **2009**, *38*, 62–72.

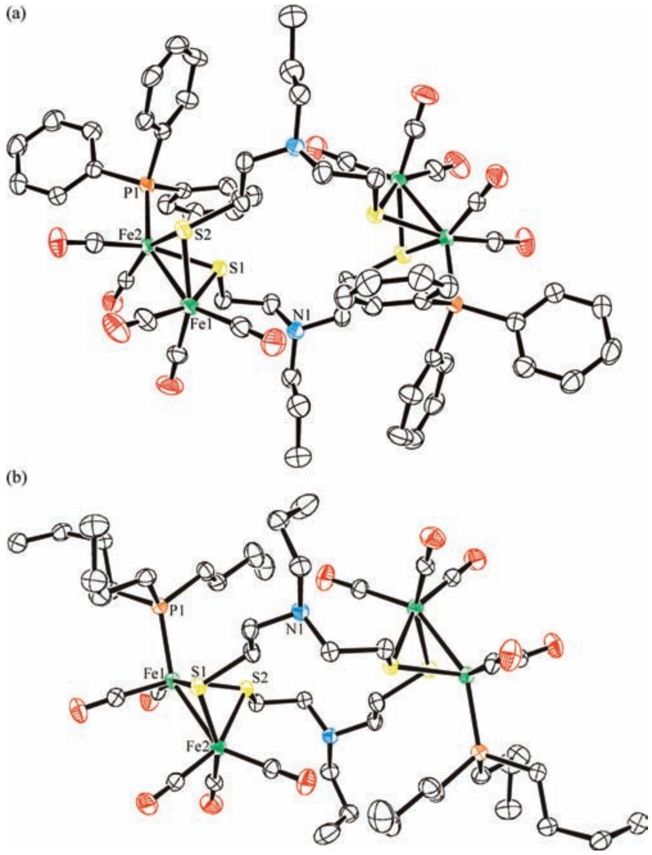

Figure 3. Molecular structures of [Fe$_2$(μ-S(CH$_2$)$_2$N^{n}Pr(CH$_2$)$_2$S)(CO)$_5$L]$_2$, (a) L = PPh$_3$, **2**; (b) L = P^{n}Bu$_3$, **3**, thermal ellipsoids drawn at 50% probability level. All hydrogen atoms are omitted for clarity. Selected bond lengths (Å) and angles (deg) for **2**: Fe$-$Fe, 2.5087(5); Fe$-$S, 2.2683; Fe$-$C$_{\mathrm{CO,ap}}$, 1.791(3); Fe$-$C$_{\mathrm{CO,ba}}$, 1.771; Fe$-$P, 2.2272(7); S$-$Fe$-$S, 79.055; S$-$Fe$-$Fe, 56.426; Fe$-$S$-$Fe, 67.150; P$-$Fe$-$S, 103.91; P$-$Fe$-$Fe, 151.89(2); for **3**: Fe$-$Fe, 2.5195(4); Fe$-$S, 2.2721; Fe$-$C$_{\mathrm{CO,ap}}$, 1.804(2); Fe$-$C$_{\mathrm{CO,ba}}$, 1.772; Fe$-$P, 2.2290(7); S$-$Fe$-$S, 80.755; S$-$Fe$-$Fe, 56.328; Fe$-$S$-$Fe, 67.345; P$-$Fe$-$S, 102.09; P$-$Fe$-$Fe, 148.84(2).

blue-shifted by about 15 cm^{-1}.[21] The *N*-protonated species are synthesized from reactions of **1a** and **2**, respectively, with strong acids such as HBF$_4$, HClO$_4$, and HOTf. The IR signals move toward higher energy by 10 cm^{-1} in accord with observation of the *N*-Me product. Deprotonation of [**1a-2H$^{\mathrm{N}}$**]$^{2+}$ and [**2$-$2H$^{\mathrm{N}}$**]$^{2+}$ by TEOA generates their parent molecules in quantitative yields.

Complexes [**1a-2Me$^{\mathrm{N}}$**]$^{2+}$, [**1a-2H$^{\mathrm{N}}$**]$^{2+}$, and [**2$-$2H$^{\mathrm{N}}$**]$^{2+}$ crystallize in the $P\overline{1}$ space group. Their structures are shown in Figure 4 as the thermal ellipsoid plot. Selected metric data are listed in the figure caption. The central nitrogen atoms of the dithiolate bridges no longer point toward the apical CO groups of the Fe$_2$S$_2$ units in all three species. The closest apical CO group is 4.489 Å away from the aza nitrogen atom among them. This result indicates no interaction between the quaternary nitrogen atom and the carbonyl carbon, which verifies the N$\cdots$C(CO$_{\mathrm{ap}}$) contacts are initiated by availability of lone pairs on the aza nitrogen atoms.

The relationship of the secondary-coordination-sphere interaction and electronic nature of the Fe$_2$ unit is further examined by comparison of **1** and **2** with the P^{n}Bu$_3$ derivative, [Fe$_2$(μ-S(CH$_2$)$_2$N^{n}Pr(CH$_2$)$_2$S)(CO)$_5$(P^{n}Bu$_3$)]$_2$, **3**, which

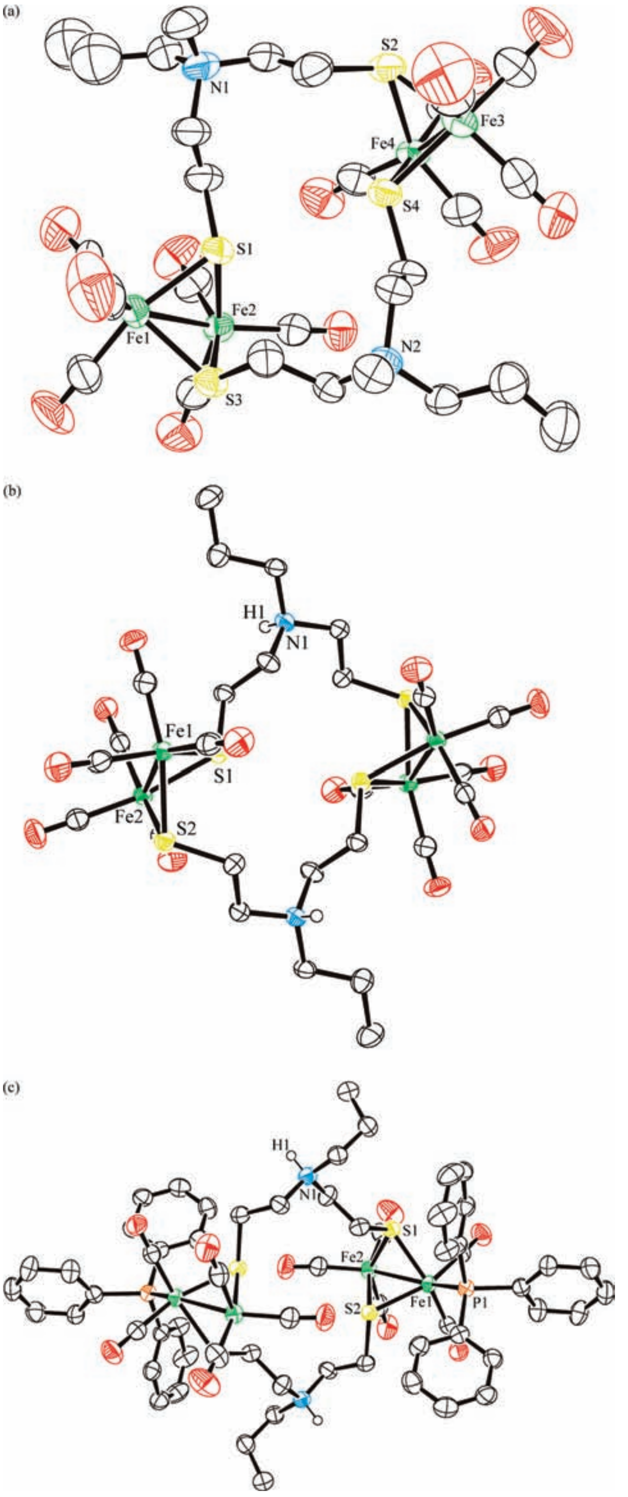

Figure 4. Molecular structures of (a) [Fe$_2$(μ-S(CH$_2$)$_2$N(Me)^{n}Pr(CH$_2$)$_2$S)(CO)$_6$]$_2$$^{2+}$, [**1a-2Me$^{\mathrm{N}}$**]$^{2+}$, thermal ellipsoids drawn at 30% probability level; (b) [Fe$_2$(μ-S(CH$_2$)$_2$N(H)^{n}Pr(CH$_2$)$_2$S)(CO)$_6$]$_2$$^{2+}$, [**1a-2H$^{\mathrm{N}}$**]$^{2+}$, thermal ellipsoids drawn at 50% probability level; (c) [Fe$_2$(μ-S(CH$_2$)$_2$N(H)^{n}Pr(CH$_2$)$_2$S)(CO)$_5$(PPh$_3$)]$_2$$^{2+}$, [**2$-$2H$^{\mathrm{N}}$**]$^{2+}$, thermal ellipsoids drawn at 30% probability level. All hydrogen except NH hydrogen atoms in all complexes are omitted for clarity. Selected bond lengths (Å) and angles (deg) for [**1a-2Me$^{\mathrm{N}}$**]$^{2+}$: Fe$-$Fe, 2.507; Fe$-$S, 2.253; Fe$-$C$_{\mathrm{CO,ap}}$, 1.794; Fe$-$C$_{\mathrm{CO,ba}}$, 1.792; S$-$Fe$-$S, 79.758; S$-$Fe$-$Fe, 56.195; Fe$-$S$-$Fe, 67.61; for [**1a-2H$^{\mathrm{N}}$**]$^{2+}$: Fe$-$Fe, 2.5312(6); Fe$-$S, 2.2587; Fe$-$C$_{\mathrm{CO,ap}}$, 1.822; Fe$-$C$_{\mathrm{CO,ba}}$, 1.803; S$-$Fe$-$S, 81.275; S$-$Fe$-$Fe, 55.923; Fe$-$S$-$Fe, 68.155; for [**2$-$2H$^{\mathrm{N}}$**]$^{2+}$: Fe$-$Fe, 2.5253(8); Fe$-$S, 2.2693; Fe$-$C$_{\mathrm{CO,ap}}$, 1.795(5); Fe$-$C$_{\mathrm{CO,ba}}$, 1.778; Fe$-$P, 2.2449(12); S$-$Fe$-$S, 80.145; S$-$Fe$-$Fe, 56.193; Fe$-$S$-$Fe, 67.615; P$-$Fe$-$S, 106.25; P$-$Fe$-$Fe, 154.49(4).

---

[21] Mejia-Rodriguez, R.; Chong, D.; Reibenspies, J. H.; Soriaga, M. P.; Darensbourg, M. Y. *J. Am. Chem. Soc.* **2004**, *126*, 12004–12014.

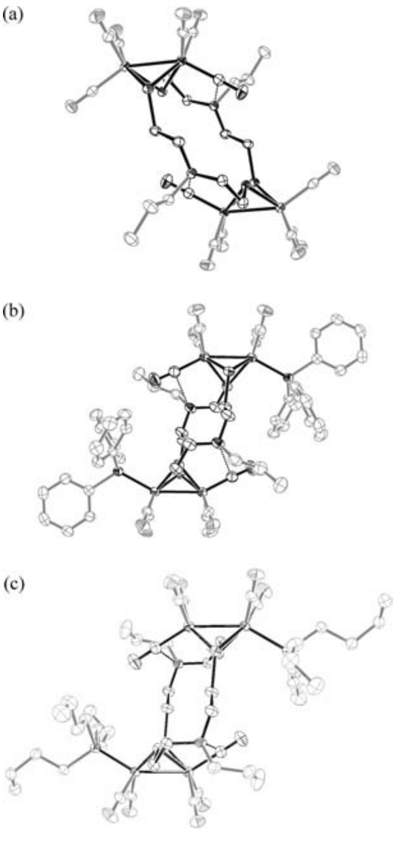

Figure 5. Representation of the closest N$\cdots$C(CO$_{ap}$) contacts in (a) **1a** (3.497 Å), (b) **2** (3.952 Å), and (c) **3** (4.040 Å). All hydrogen atoms are omitted for clarity. The organic substituents of the phosphines and the carbonyls are in gray shade. Only the apical carbonyl groups involved are highlighted.

has a similar structure as **2**, shown in Figure 3. The N$\cdots$C(CO$_{ap}$) distance increases from 3.497 Å in **1a** to 3.952 Å in **2**. When the CO group within the {Fe$_2$(CO)$_6$} moiety is substituted by P^{n}Bu$_3$ instead of PPh$_3$, this distance is increased to 4.040 Å in **3**. Figure 5 displays these three species, showing the aza nitrogen sites consistently point the lone pairs toward the apical carbonyl carbons in all three complexes. Since P^{n}Bu$_3$ is a stronger σ-donor (substituent contribution $\chi_i = 1.4$; for PX$_1$X$_2$X$_3$: ν (cm^{-1}) $= 2056.1 + \sum\chi_i$) with a smaller cone angle ($\theta = 132°$) than PPh$_3$ ($\chi_i = 4.3, \theta = 145°$),[22] the extended N$\cdots$C(CO$_{ap}$) distance of **3** is the result from the greatly electronically enriched Fe centers. In addition, the steric effect of the phosphines is considered to make the minimal contribution to the N$\cdots$C(CO$_{ap}$) distance since the interaction occurs at the structurally unhindered Fe(CO)$_3$ moiety. It is said that the N$\cdots$C(CO$_{ap}$) distance is a dynamic measure of the electronic nature of the Fe$_2$ moiety. Figure 6 shows the molecular structure of the CH$_2$ analogue, [Fe$_2$(μ-S(CH$_2$)$_5$S)(CO)$_6$]$_2$, **4**. The structural parameters do not show any exception.

Electrochemistry. In the absence of a proton source, the cyclic voltammogram of **1a** in the accessible electrochemical window of CH$_2$Cl$_2$ under N$_2$ at room temperature exhibits one irreversible reduction step at -1.90 V (all potentials in this paper are vs Fc/Fc$^+$) (Figure 7a). This reduction wave consists of two electrochemical responses, which could be disentangled when the voltammogram was measured in tetrahydrofuran (THF).[23] Reversibility of the reduction events is improved at low temperature or at the fast scan rate (Supporting Information, Figure *S3*). When the solution was purged with CO for a period of time, the voltammogram for **1a** in CH$_2$Cl$_2$ at $v = 100$ mV s^{-1} under 1 atm CO gas did not reveal any reversibility for all electrochemical processes at room temperature (RT). Voltammetric responses of the decomposed species are observed at about 700 mV more negative potential. Such electrochemical behavior has been observed in the SEt analogue.[24] Structural rearrangement resulted from rupture of the Fe$-$S bond or loss of CO upon reduction of **1a** could be responsible for formation of the daughter products.[25,26]

The electrocatalytic activity of **1a** was monitored under N$_2$ with stepwise addition of HOAc. The study of electrocatalysis was performed in CH$_2$Cl$_2$ for the purpose of comparison because complexes listed in this report have the best solubility in CH$_2$Cl$_2$, which can avoid any incorrect measurement of the peak current for each reduction in the course of acid addition. Background proton reduction in the absence of complexes was performed on account of the comparison.[27] No detectable voltammetric responses of HOAc are observed within the accessible electrochemical window of CH$_2$Cl$_2$, suggesting any electrocatalytic proton formation can only proceed under the presence of catalysts.

None of all reported diiron azadithiolate carbonyl complexes yields the *N*-protonated products when HOAc is used as the proton source. Neither does complex **1a**. Electrocatalytic H$_2$ production from HOAc by the biomimetic catalyst is then expected to have no involvement of the protonated aza nitrogen species. When electrocatalysis of **1a** was monitored with titration of HOAc, a reduction wave was observed at the slightly more positive potential (-1.84 V), and the remainder of the cyclic voltammograms do not appear to show any significant influence, as shown in Figure 7a. The peak current of this reduction event shows the linear relationship with sequential increments of acid added, indicating electrocatalytic H$_2$ production occurs at this potential.[26,28] When the current function $i_p/v^{1/2}$ for this reduction is measured in the presence of 2 equiv of HOAc, non-linearity dependence at slow scan rates is obtained, indicative of the ECE catalytic steps (Supporting Information, Figure *S4*).[29] Since protonation does not occurs at the aza nitrogen site during electrocatalysis, it is reasonable to propose that catalytic steps of hydrogen evolution by **1a** involve the direct protonation to the Fe center, which is initiated

---

(22) Tolman, C. A. *Chem. Rev.* **1977**, *77*, 313–348.

(23) Zeng, X.; Li, Z.; Xiao, Z.; Wang, Y.; Liu, X. *Electrochem. Commun.* **2010**, *12*, 342–345.

(24) Borg, S. J.; Ibrahim, S. K.; Pickett, C. J.; Best, S. P. *C. R. Chim.* **2008**, *11*, 852–860.

(25) (a) Darchen, A.; Mousser, H.; Patin, H. *J. Chem. Soc., Chem. Commun.* **1988**, 968–970. (b) Borg, S. J.; Tye, J. W.; Hall, M. B.; Best, S. P. *Inorg. Chem.* **2007**, *46*, 384–394.

(26) Felton, G. A. N.; Vannucci, A. K.; Chen, J.; Lockett, L. T.; Okumura, N.; Petro, B. J.; Zakai, U. I.; Evans, D. H.; Glass, R. S.; Lichtenberger, D. L. *J. Am. Chem. Soc.* **2007**, *129*, 12521–12530.

(27) Felton, G. A. N.; Glass, R. S.; Lichtenberger, D. L.; Evans, D. H. *Inorg. Chem.* **2006**, *45*, 9181–9184.

(28) Bhugun, I.; Lexa, D.; Savéant, J.-M. *J. Am. Chem. Soc.* **1996**, *118*, 3982–3983.

(29) Bard, A. J.; Faulkner, L. R. *Electrochemical Methods: Fundamentals and Applications*; John Wiley & Sons: New York, 1980.

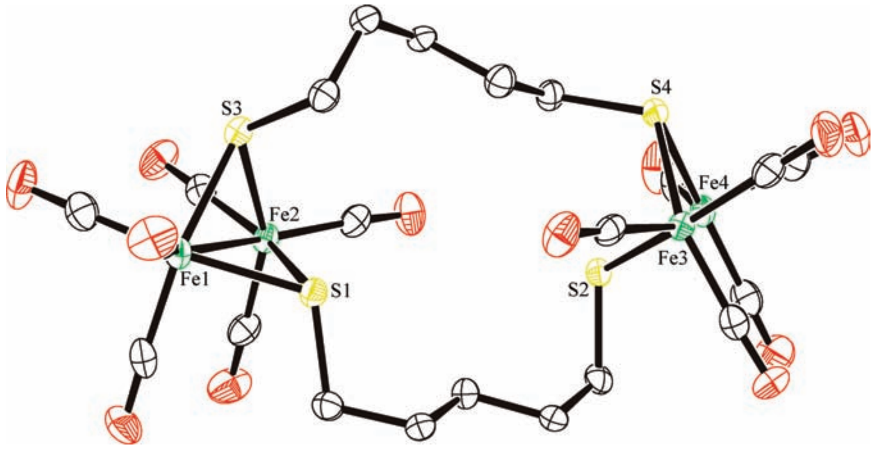

Figure 6. Molecular structure of $[Fe_2(\mu\text{-}S(CH_2)_5S)(CO)_6]_2$, **4**, thermal ellipsoids drawn at 50% probability level. All hydrogen atoms are omitted for clarity. Selected bond lengths (Å) and angles (deg): Fe−Fe, 2.5001; Fe−S, 2.2659; $Fe-C_{CO,ap}$, 1.8078; $Fe-C_{CO,ba}$, 1.7879; S−Fe−S, 80.058; S−Fe−Fe, 56.505; Fe−S−Fe, 66.993.

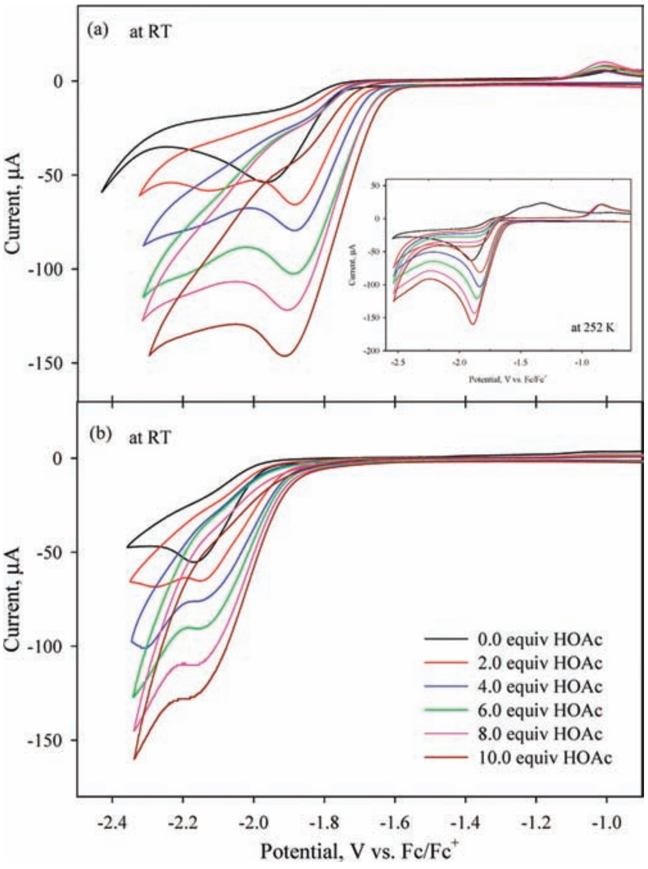

Figure 7. Cyclic voltammograms of (a) **1a** (1 mM) and (b) **2** (1 mM) with increments of HOAc (0.0, 2.0, 4.0, 6.0, 8.0, 10.0 equiv) in CH_2Cl_2 (v = 100 mV s^{-1}, 0.1 M $n\text{-}Bu_4NPF_6$). The inset shows the cyclic voltammograms of **1a** recorded at 252 K (v = 400 mV s^{-1}, 0.4 M $n\text{-}Bu_4NPF_6$), revealing quasi-reversibility ($i_p^a/i_p^c \approx 0.6$) of the reduction in **1a** at this temperature. It also confirms the voltammetric response at ~ -2.15 V in the presence of 2.0 equiv of HOAc at RT corresponds to the daughter product of the reduced **1a** species.

Scheme 1

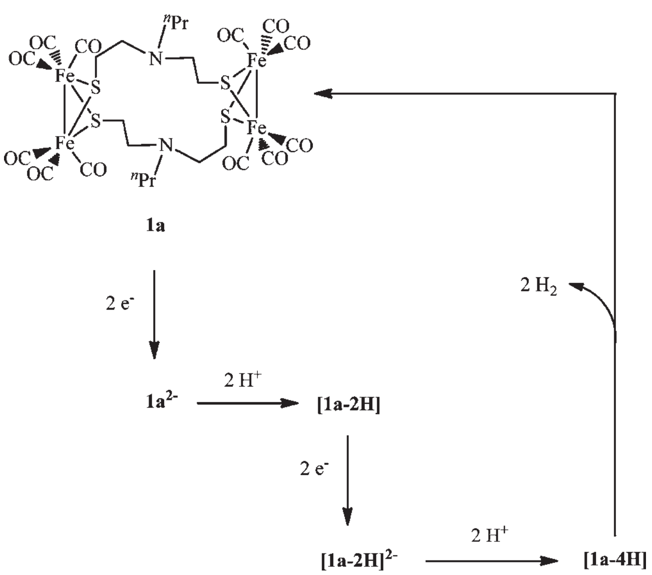

by the reduction process.[26,30] Supporting Information, Figure *S5* shows that disappearance of the anionic response of the primary reduction is accompanied with appearance of the electrocatalytic wave at the potential near the first reduction. The ECEC mechanism displayed in Scheme 1 is therefore proposed for **1a**.[31] The starting material is reduced first. Rapid protonation of the reduced product, $\mathbf{1a}^{2-}$ ($\equiv [\{Fe^0Fe^I\}^-]_2$), is accounted for the positive potential shift. A consecutive reduction follows to generate the second reduced intermediate, $[\mathbf{1a\text{-}2H}]^{2-}$. It then reacts with protons to form the proposed transient (η_2-H_2)FeFe species which releases H_2 to resume the starting molecule **1a**. This catalytic mechanism is surprisingly identical to that proposed for the phosphine-substituted species in the current study. The mechanistic discrepancy between the ECEC processes by **1a** and the EECC processes by its all-CO analogues, $Fe_2(\mu\text{-}SS)_2(CO)_6$ (SS = SEt, pdt, adt),[32,33] occurs in that an

---

(30) Charreteur, K.; Kdider, M.; Capon, J.-F.; Gloaguen, F.; Pétillon, F. Y.; Schollhammer, P.; Talarmin, J. *Inorg. Chem.* **2010**, *49*, 2496–2501.

(31) Borg, S. J.; Behrsing, T.; Best, S. P.; Razavet, M.; Liu, X.; Pickett, C. J. *J. Am. Chem. Soc.* **2004**, *126*, 16988–16999.

(32) Chong, D.; Georgakaki, I. P.; Mejia-Rodriguez, R.; Sanabria-Chinchilla, J.; Soriaga, M. P.; Darensbourg, M. Y. *Dalton Trans.* **2003**, 4158–4163.

(33) Liu, T.; Wang, M.; Shi, Z.; Cui, H.; Dong, W.; Chen, J.; Åkermark, B.; Sun, L. *Chem.—Eur. J.* **2004**, *10*, 4474–4479.

electronic structure of Fe^0Fe^0 is required for the latter prior to protonation of the Fe site but the Fe^0Fe^I state of **1a** is already electron rich enough to attract protons. Very recently, one example of an all-CO analogue able to catalyze the proton reduction from mild acids at a potential near the primary electron-transfer process was reported.[30]

The experimental results and theoretical studies have shown that the lowest unoccupied molecular orbital (LUMO) and the highest occupied molecular orbital (HOMO) of the diiron dithiolate complex has significant Fe−Fe character.[32,34] In other words, replacement of CO by phosphines can make a direct contribution to the metal-based voltammetric response. When one of the CO groups within the $\{Fe_2(CO)_6\}$ moiety in **1a** is substituted by PR_3, the reduction wave shifts from −1.9 V of **1a** to −2.17 and −2.32 V for **2** and **3**, respectively in the absence of HOAc (Figure 7b and Supporting Information, Figure *S6*). The cathodic shift of 270 and 420 mV reflects increase of electron density about the Fe center upon substitution of the better π-acid ligand, CO, by phosphines as a result of increased difficulty to reduce the metal site. For different donating ligands such as PMe_3, the similar influence has been observed.[5,10,35] With addition of HOAc, the electrocatalytic response is observed at −2.11 and −2.25 V for **2** and **3**, respectively. Hydrogen production is then proposed to go via the similar ECEC mechanism. Since electrocatalysis in HOAc for complexes **1a**, **2**, and **3** runs through the same mechanism, the electron-richer environment about the iron sites in **1a** than that in other all-CO analogues could be proposed, which is already hinted by its red-shifted FTIR bands.

Influence of the Bridgehead. Involvement of the aza nitrogen bridgehead in electrocatalysis of HOAc can be examined via either substitution of the NR sites with the CH_2 groups or blocking availability of the lone pairs. Cyclic voltammogram of **4** in the accessible electrochemical window of CH_2Cl_2 under N_2 at room temperature exhibits one irreversible reduction step at −1.97 V under the acid-free condition (Figure 8a). Low temperature and fast scan rates can improve reversibility of the cathodic wave (Supporting Information, Figure *S7*). Upon contact with HOAc, an electrocatalytic response appears at the potential near the reduction. Supporting Information that protonation occurs after the primary reduction event is displayed in Supporting Information, Figure *S8*. The ECEC mechanism same with that for **1a** is then proposed for **4**. From approximately same current height of the electrocatalytic response for both **1a** and **4**, the aza nitrogen site plays a non-important role during proton reduction from HOAc.

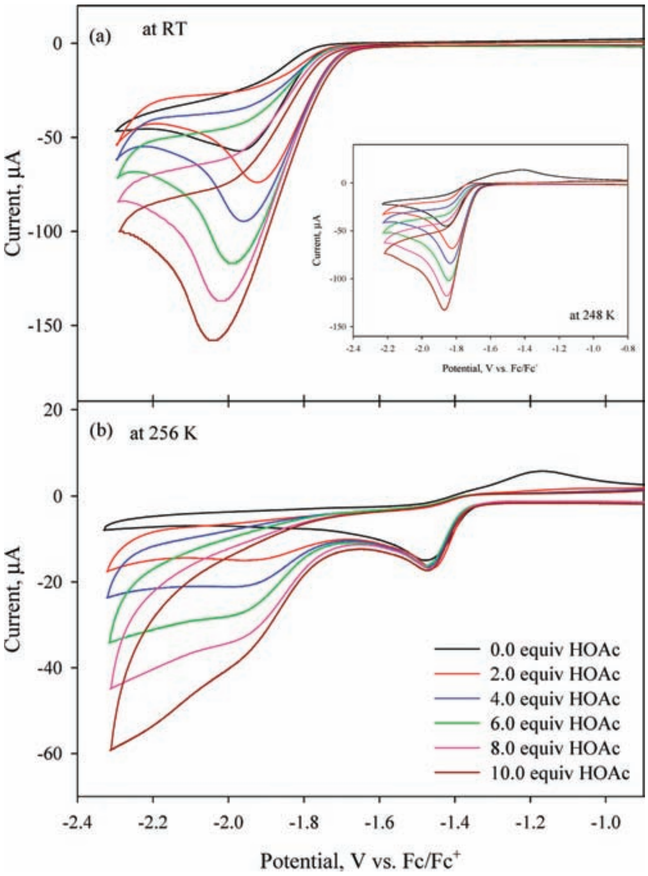

Figure 8. Cyclic voltammograms of (a) **4** (1 mM, RT, $\upsilon = 100$ mV s^{-1}, 0.1 M n-Bu_4NPF_6) and (b) $[\mathbf{1a\text{-}2Me^N}]^{2+}$ (1 mM, 256 K, $\upsilon = 200$ mV s^{-1}, 0.4 M n-Bu_4NPF_6) with increments of HOAc (0.0, 2.0, 4.0, 6.0, 8.0, 10.0 equiv) in CH_2Cl_2. The inset shows the low-temperature cyclic voltammograms of **4**, revealing quasi-reversibility of the first reduction at 248 K ($\upsilon = 200$ mV s^{-1}, 0.4 M n-Bu_4NPF_6).

This statement is supported by the electrochemical studies of $[\mathbf{1a\text{-}2H^N}]^{2+}$ and $[\mathbf{2{-}2H^N}]^{2+}$ where two irreversible reduction waves are observed each in their voltammograms, displayed in Supporting Information, Figure *S9*. The first reduction is recorded at −1.41 and −1.66 V for $[\mathbf{1a\text{-}2H^N}]^{2+}$ and $[\mathbf{2{-}2H^N}]^{2+}$, respectively. It is the EC response involved with the conversion of the NH species to the parent molecules. The second reduction measured at −1.85 V and −2.07 V for $[\mathbf{1a\text{-}2H^N}]^{2+}$ and $[\mathbf{2{-}2H^N}]^{2+}$, respectively, is the electrochemical process of **1a** and **2**, respectively. The assignment is based on electrolysis of HOAc by $[\mathbf{1a\text{-}2H^N}]^{2+}$, monitored by in situ IR spectroscopy. The infrared signatures of $[\mathbf{1a\text{-}2H^N}]^{2+}$ diminish in association with appearance of those of **1a** without consumption of HOAc in the initial stage, shown in Supporting Information, Figure *S9c*. This suggests that only electrolysis of $[\mathbf{1a\text{-}2H^N}]^{2+}$ occurs at first. The passage of charge is 2.1 F mol^{-1} of $[\mathbf{1a\text{-}2H^N}]^{2+}$, which is in agreement with the expected value for generation of **1a** and 1 equiv of H_2. Once depletion of $[\mathbf{1a\text{-}2H^N}]^{2+}$ to **1a** is completed, substantial decrease of HOAc is observed, accompanied by gradual increase of the decomposed species, which is discussed later, throughout the course of electrolysis.

Since the nitrogen factor has been excluded, the scope of the electrochemical study of $[\mathbf{1a\text{-}2Me^N}]^{2+}$ can be narrowed down to the electronic factor, that is, the influence of methylation on the electronic property of the Fe_2 centers. The *N*-methylated species of **1a** contains positively charged N atoms, which have a strongly electron-withdrawing effect. The cyclic voltammogram of $[\mathbf{1a\text{-}2Me^N}]^{2+}$ shows a reduction wave at −1.44 V under the acid-free condition (Figure 8b). Reversibility of the redox

---

[34] Hall, M. B.; Fenske, R. F.; Dahl, L. F. *Inorg. Chem.* **1975**, *14*, 3103–3117.

[35] (a) Thomas, C. M.; Rüdiger, O.; Liu, T.; Carson, C. E.; Hall, M. B.; Darensbourg, M. Y. *Organometallics* **2007**, *26*, 3976–3984. (b) Si, Y.; Ma, C.; Hu, M.; Chen, H.; Chen, C.; Liu, Q. *New J. Chem.* **2007**, *31*, 1448–1454. (c) Gao, W.; Ekströem, J.; Liu, J.; Chen, C.; Eriksson, L.; Weng, L.; Åkermark, B.; Sun, L. *Inorg. Chem.* **2007**, *46*, 1981–1991.

event can be restored at low temperature and at the fast scan rate (Supporting Information, Figure *S10*). This voltammetric response at 256 K shows a slight increase in current height ($i_{pc}{}^{acid}/i_{pc}{}^{acid\text{-}free} < 1.2$) as the acid concentration is increased. The current increase is attributed to the daughter product resulted from the reductions (vide infra). On the other hand, a new electrochemical process at −1.88 V reveals significant changes (Figure 8b). Since the potential of this electrocatalytic reduction in [**1a-2Me**^{N}]$^{2+}$ is very close to that (−1.84 V) in **1a**, it is suspected that demethylation might occur upon the reduction at −1.44 V.[21] The CH_2Cl_2 solution of [**1a-2Me**^{N}]$^{2+}$ in the presence of HOAc was subject to exhaustive electrochemical cycles, and the resultant solution was vacuumed to dryness. No IR signal of **1a** in the hexane extract was evidenced. It is concluded that demethylation of [**1a-2Me**^{N}]$^{2+}$ to **1a** does not occur.

The suspected catalytic process at −1.44 V is authenticated to combination of the E (electrochemical) event of [**1a-2Me**^{N}]$^{2+}$ and the EC (electrochemical-chemical) event involved with the decomposed species, which is concluded based on the following results. First of all, when the cyclic voltammogram of [**1a-2Me**^{N}]$^{2+}$ is recorded in the presence of 2 equiv of HOAc at room temperature, the peak current of the reduction event at −1.44 V in CH_2Cl_2 is approximately 1.7 times that measured under the acid-free condition. More acids only cause minimal increase in current height afterward. If this current increase was indicative of the electrocatalytic process related to [**1a-2Me**^{N}]$^{2+}$, the peak current would change with increase of scan rates, assuming that the electron transfer process is diffusion controlled. In contrast, when the scan rate is increased, the difference of the current height for the acid-free and acidic (4 equiv of HOAc) conditions decreases. At $v = 40\ V\ s^{-1}$, both peak currents overlap (Supporting Information, Figure *S11*). Second, when electrocatalytic measurement of [**1a-2Me**^{N}]$^{2+}$ is performed at 261 K, the peak current of the first reduction event in CH_2Cl_2 decreases to 1.2 times that measured in the absence of acids. Third, intensity of ν(COO) bands remains unchanged in the course of bulk electrolysis of [**1a-2Me**^{N}]$^{2+}$ at −1.65 V in the presence of HOAc at 255 K. The results, therefore, suggest that any catalytic reaction that occurred at −1.44 V is not related to [**1a-2Me**^{N}]$^{2+}$. Instead, its increased current height at the RT electrolysis is due to the catalytic event involved with the daughter product originated from the reduced species, [**1a-2Me**^{N}]. Suppression of this decomposed species is achieved at low temperature and at the fast scan rate.

Non-linearity dependence at slow scan rates is obtained for the current function $i_p/v^{1/2}$ of the reduction at −1.88 V in the presence of 2 equiv of HOAc (Supporting Information, Figure *S12*). This indicates the ECE catalytic steps occur at the potential. In addition, protonation occurs only when the Fe^0Fe^0 state is achieved, suggesting electron density about the Fe center is perturbed owing to methylation. From the electronic spectra of **1a** and [**1a-2Me**^{N}]$^{2+}$, one can anticipate that introduction of positive charges to the molecule does not alter the frontier orbitals but decreases the energetics of the MOs ($\Delta E = 0.46$ V), which makes the unoccupied ones electrochemically more accessible (Supporting Information, Figure *S13*). In return, it is more difficult to reduce protons by the valence electrons. The results suggest that the electron structure of the Fe_2 unit dictates the catalytic mechanism under the HOAc condition.

Spectroelectrochemistry. During electrocatalysis of HOAc (50 equiv) by **1a** at −2.1 V in CH_2Cl_2 at 266 K, monitored by in situ IR spectroscopy, the infrared signatures of **1a** remain intact as HOAc is consumed, as shown in Figure 9a. In contrast, both of the IR signals of **1a** and HOAc decrease simultaneously when the similar experiment is performed at room temperature. A new species is gradually formed, whose IR bands resemble those of the reduction product of **1a** electrochemically prepared in the absence of acids, Figure 9b. This reduction species, **5**, features the ν(CO) bands of 2024, 1973, 1936, 1925, and 1719 cm^{-1} that are closely similar to those of the diiron species, proposed by Pickett and Best, with bridging CO and thiolate groups in which the thiolate bridge has one pendent end.[31] The structure of **5** is also possibly related to the calculated model where one of the Fe centers has an inverted geometry with a semibridging carbonyl via rupture of the Fe−S bond.[25,26] It is reasonable to propose the followings. First of all, the complex **1a**$^{2-}$ is a transient species. Protonation of **1a**$^{2-}$ upon the first reduction is a fast step. This protonation process is also an essential step to retain electrocatalytic efficiency of **1a** toward reduction of HOAc. Second, the chemical reaction, possibly depletion of **1a**$^{2-}$ to **5**, becomes competitive at room temperature, which is observed in the RT electrocatalysis.

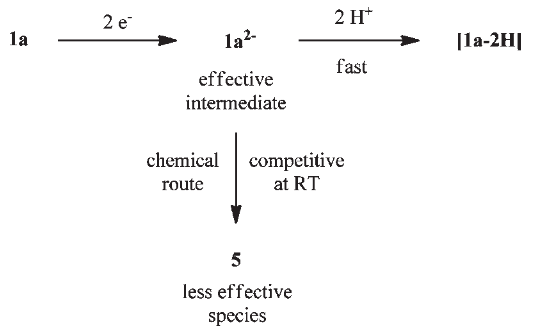

The pdt analogue of **5** has been proposed to kinetically slowly react with acids.[31] Our results also reach the same conclusion: **5** is the less effective catalyst than **1a**$^{2-}$. Figure 9c displays the Q-t plot for both RT and LT electrolysis of **1a** in the presence of HOAc. The linear dependence of Q-t is obtained in the first 3600 s for both, which leads to 4.1 and 2.9 $mol^{-1}\ h^{-1}$ of the turnover numbers (TONs) in CH_2Cl_2 for RT and 266 K, respectively. The lower TON at 266 K is understandable by the lower conductivity at LT. For the LT electrolysis, the linear dependence is kept for the first 10000 s until acids are almost exhausted. In contrast, the curve of the RT electrolysis starts to deviate from linearity at about 4000 s. Decrease of the catalytic efficiency is reasoned by the poor activity of **5** originated from **1a**$^{2-}$, as shown in Figure 9b. For [**1a-2Me**^{N}]$^{2+}$, similar results are yielded, shown in Supporting Information, Figure *S14*. 1.9 and 1.8 $mol^{-1}\ h^{-1}$ of the TONs in CH_2Cl_2 for RT and 259 K, respectively, are estimated.

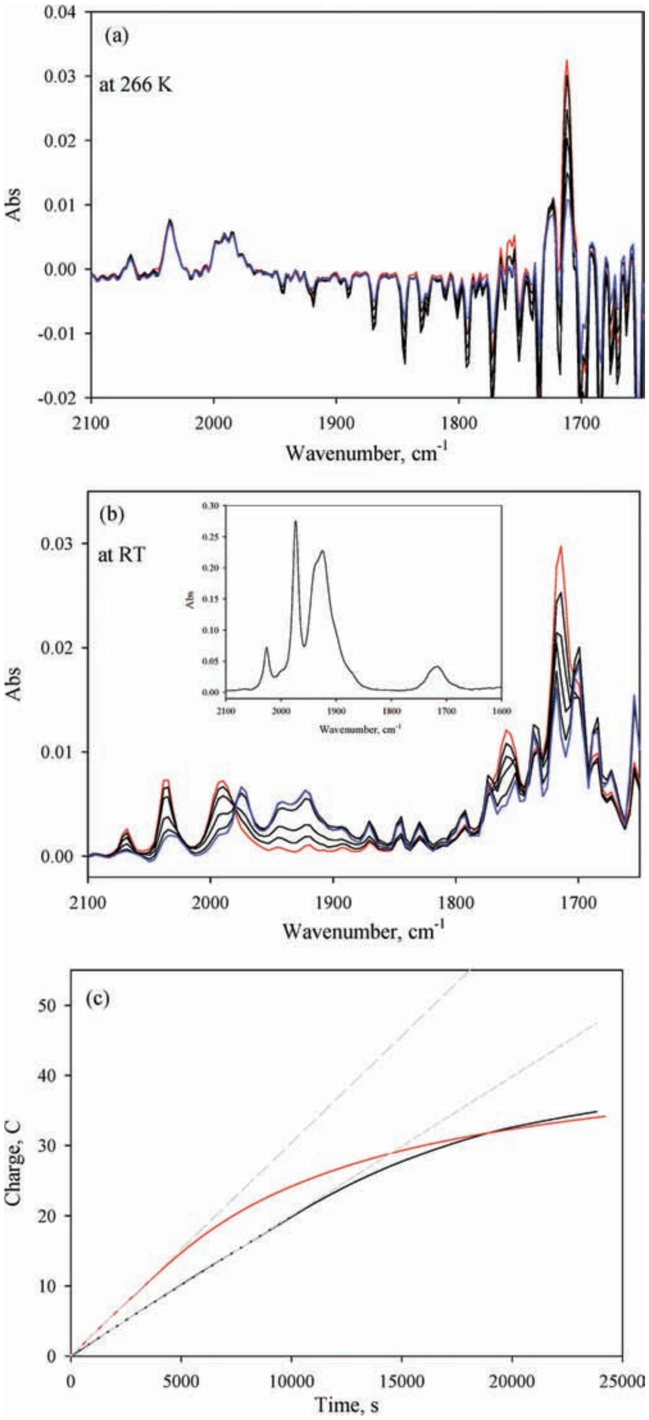

Figure 9. (a) In situ IR spectra recorded during electrocatalysis of HOAc by $[Fe_2(\mu\text{-}S(CH_2)_2N^nPr(CH_2)_2S)(CO)_6]_2$, **1a**, in CH_2Cl_2 under N_2 at 266 K. The solid line in red represents ν(CO) of **1a** in the presence of 50 equiv of HOAc prior to electrolysis. The solid line in blue represents ν(CO) of **1a** in the latter stage, indicating the catalyst does not deplete as HOAc (ν(COO) = 1711 cm^{-1}) is consumed during electrocatalysis. (b) The RT in situ IR spectra. The inset shows the IR spectrum of **5**, resulted from bulk electrolysis of **1a** in CH_2Cl_2 in the absence of acids. (c) The Q-t plot for the LT (in black) and RT (in red) electrolysis. The gray dash lines show extrapolation of the linear dependence at the initial catalytic rate.

Concluding Remarks

In the pdt and adt derivatives of diiron model complexes, a separation of ~3.2 Å has been measured between the X atom of the S−C−X−C−S linker and the carbonyl carbon. Such short distance is commonly assumed to be due, in major part, to structural strain of the dithiolate bridges. Involvement of electronic distribution probably plays a minor counterpart. In contrast, the dithiolate ligands from complexes of $[Fe_2(\mu\text{-}S(CH_2)_2NR(CH_2)_2S)(CO)_{6-x}L_x]_2$ (R = ^{n}Pr, x = 0, **1a**; R = ^{i}Pr, x = 0, **1b**; R = ^{n}Pr, L = PPh_3, x = 1, **2**; R = ^{n}Pr, L = P^nBu_3, x = 1, **3**) do not face the same structural strain. Azadiethylenethiolate that is a saturated S−S linker with high flexibility spans between two $\{Fe_2(CO)_6\}$ fragments in **1**−**3**. For them to adapt a distorted configuration where the aza nitrogen is oriented to have its lone pair pointing toward the apical carbonyl carbon, back-bonding experienced by CO from the metal site is certainly not enough. In other words, the Fe center is relatively electron-deficient. This is the reason why protonation can not proceed onto the Fe−Fe vector to give the Fe-hydride species.

Since the distance of the N···C(CO_{ap}) contact is not predominately structure dependent, its variation can be treated as a dynamic measure of the electronic nature of the Fe_2 core. It is observed that the distance increases (3.497 (**1a**) vs 3.952 (**2**) vs 4.040 Å (**3**)) when one CO group within the $\{Fe_2(CO)_6\}$ moiety is substituted by PPh_3 or P^nBu_3. The result implies the negative correlation between this intramolecular interaction and electron density about the Fe centers. In addition, the result tentatively suggests that the aza nitrogen site could serve as a stabilizing factor in the thermodynamic aspect. If the proposed enzymatic mechanism of formation of Fe-hydride involves a bridging hydride intermediate, it could have generated from the transient terminal hydride species via intramolecular rearrangement.[7,36] This process causes the then bridging CO to be placed in the terminal fashion as well as to experience less back-donation from the now Fe^{II} center. It is expected that the presence of the weak N···C(CO_{ap}) interaction, which forms five-membered rings, shall assist stabilization of the CO on the catalytic Fe site. This is consistent with the results from DFT calculations revealing that strong interaction of the central bridgehead with the apical CO or the iron center leads to the minimum energy $Fe_2(\mu\text{-}SS)(CO)_6$ structure.[8]

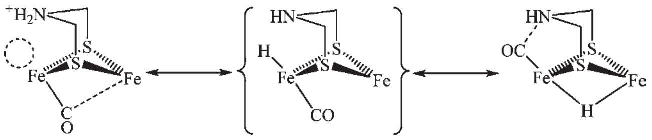

From the literature survey, it is found that addition of two electrons is necessary for every all-CO species prior to proton uptake in the presence of HOAc. These EE processes that generate the electron enriched Fe^{0}Fe^0 centers to facilitate protonation by HOAc are essential for initiation of the catalytic cycles. In contrast, protonation by HOAc occurs after the Fe^{0}Fe^I level of **1a** and **4** is reached, which indicates that the ECEC mechanism proposed for the phosphine derivatives, **2** and **3**, is applied to both of **1a** and **4**. The determining factor for such mechanism is the presence of the Fe_2 core with increased basicity, which has been evidenced by IR signals. The ν(CO) bands of both complexes are shifted to

---

(36) (a) Barton, B. E.; Rauchfuss, T. B. *Inorg. Chem.* **2008**, *47*, 2261–2263. (b) Orain, P.-Y.; Capon, J.-F.; Kervarec, N.; Gloaguen, F.; Pétillon, F.; Pichon, R.; Schollhammer, P.; Talarmin, J. *Dalton Trans.* **2007**, 3754–3756. (c) Ezzaher, S.; Capon, J.-F.; Gloaguen, F.; Pétillon, F. Y.; Schollhammer, P.; Talarmin, J.; Pichon, R.; Kervarec, N. *Inorg. Chem.* **2007**, *46*, 3426–3428.

lower energy. On the other hand, protonation onto the Fe^0Fe^0 state instead of the Fe^0Fe^I state occurs in **[1a-2Me^N]$^{2+}$** while the aza nitrogen sites are methylated, and the strongly electron-withdrawing effect is exerted. The results suggest that the electron structure of the Fe_2 unit dictates the electrocatalytic mechanism under the HOAc condition. Further experimental and theoretical investigations on the relationship of electronic structure of the Fe_2 core and the catalytic mechanism are in progress.

Experimental Section

General Methods. All reactions were carried out by using standard Schlenk and vacuum-line techniques under an atmosphere of purified nitrogen. All commercial available chemicals were of ACS grade and used without further purification. Solvents were of HPLC grade and purified as follows: diethyl ether and THF were distilled from sodium/benzophenone under N_2. Hexane was distilled from sodium under N_2. Dichloromethane was distilled from CaH_2 under N_2. Acetonitrile was distilled first over CaH_2 and then from P_2O_5 under N_2. Deuterated solvents obtained from Merck were distilled over 4 Å molecular sieves under N_2 prior to use. $RN(CH_2CH_2SH)_2$ (R = ^{n}Pr, ^{i}Pr) were prepared according to related literature procedures.[37]

Infrared spectra were recorded on a Perkin-Elmer Spectrum One using a 0.05-mm CaF_2 cell. ^1H, $^{13}C\{^1H\}$ and $^{31}P\{^1H\}$ NMR spectra were recorded on a Bruker AV-500 or DRX-500 spectrometer operating at 500, 125.7, and 202.49 MHz, respectively. UV−vis spectra were recorded on a Varian Cary 5000 spectrophotometer using 1-cm cuvettes fitted with Teflon stoppers. Mass spectral analyses were done on a Waters LCT Premier XE at Mass Spectrometry Center in the Institute of Chemistry, Academia Sinica. Elemental analyses were performed on an Elementar vario EL III elemental analyzer.

Electrochemistry. Electrochemical measurements were recorded on a CH Instruments 630C electrochemical potentiostat using a gastight three-electrode cell under N_2 at room temperature or at the specific temperature mentioned. A glassy carbon electrode and a platinum wire were used as working and auxiliary electrodes, respectively. The reference electrode was a non-aqueous Ag/Ag^+ electrode (0.01 M $AgNO_3$/0.1 M $n\text{-}Bu_4NPF_6$ or 0.4 M $n\text{-}Bu_4NPF_6$). All potentials are measured in 0.1 or 0.4 M $n\text{-}Bu_4NPF_6$ solution in CH_2Cl_2 or THF. They are reported against ferrocene/ferrocenium (Fc/Fc^+). For electrocatalytic study of hydrogen production, increments of acids were added by microsyringe. Analysis of gas evolved from the electrochemical processes by GC (Agilent 6890 gas chromatograph with a TCD detector and a Supelco Carboxen 1000 column. Argon was used as the carrier gas) confirms hydrogen to be the sole content in the gaseous product.

Spectroelectrochemistry was performed by a Mettler Toledo ReactIR iC10 in situ FTIR system equipped with a MCT detector and a 0.625-in. SiComp probe. Graphite rods (6.15 mm in diameter) were used as working and auxiliary electrodes. Reference electrode was a non-aqueous Ag/Ag^+ electrode (0.01 M $AgNO_3$/0.1 M $n\text{-}Bu_4NPF_6$), which was placed in a separated compartment with a fine porosity glass frit. The solution was stirred under N_2 throughout bulk electrolysis.

Molecular Structure Determinations. The X-ray single crystal crystallographic data collections for **1a**, **1a$_{asym}$**, **1b**, **2**, **3**, **[1a-2Me^N]$^{2+}$**, **[1a-2H^N]$^{2+}$**, **[2−2H^N]$^{2+}$**, and **4** were carried out at 150, 293, or 295 K on a Bruker SMART APEX CCD four-circle diffractometer with graphite-monochromated Mo Kα radiation (λ = 0.71073 Å) outfitted with a low-temperature, nitrogen-stream aperture. The structures were solved using direct methods, in conjunction with standard difference Fourier techniques and refined by full-matrix least-squares procedures. A summary of the crystallographic data for complexes **1a**, **1a$_{asym}$**, **1b**, **2**, **3**, **[1a-2Me^N]$^{2+}$**, **[1a-2H^N]$^{2+}$**, **[2−2H^N]$^{2+}$**, and **4** is shown in Supporting Information, Table *S1*. An empirical absorption correction (multiscan) was applied to the diffraction data for all structures. All non-hydrogen atoms were refined anisotropically, and all hydrogen atoms were placed in geometrically calculated positions by the riding model. All software used for diffraction data processing and crystal structure solution and refinement are contained in the SHELXL-97 program suites.[38] The propyl group, C(18), C(19), C(20), of the quaternary amine is disordered with the methyl group, C(17) in **[1a-2Me^N]$^{2+}$**. The chlorine atoms, Cl(2) and Cl(8), from two of the co-crystallized CH_2Cl_2 molecules exhibit disorder.

Synthesis of [$Fe_2(\mu\text{-}S(CH_2)_2N^{n}Pr(CH_2)_2S)(CO)_6]_2$, 1a. Preparation of this complex but not its structure was previously reported.[5] A solution of $Fe_3(CO)_{12}$ (1.0 g, 1.98 mmol) in THF (20 mL) was treated with $^nPrN(CH_2CH_2SH)_2$ (394 mg, 2.2 mmol). The reaction mixture was then stirred at refluxing temperature for 30 min. The resulting brown-red mixture was evaporated to dryness in vacuo, and the crude product was purified by chromatography on silica gel with CH_2Cl_2/hexane (v/v 1/1) as the eluent. From the red band, **1a** (145 mg, 16%) was obtained as a red solid. Two kinds of red crystals were grown from hexane at −20 °C. Crystallographic structural characterization confirmed these crystals to have the same structures but in two different space group systems, $P2_1/c$ and $P2_1/n$ for **1a** and **1a$_{asym}$**, respectively. IR (hexane, cm^{-1}): ν_{CO} 2069 (m), 2037 (vs), 1999 (s), 1988 (s). ^1H NMR (500 MHz, $CDCl_3$): 0.88 (t, $^3J_{HH}$ = 7.3 Hz, 6H, $CH_2CH_2CH_3$), 1.50 (sext, $^3J_{HH}$ = 7.5 Hz, 4H, $CH_2CH_2CH_3$), 2.34 (t, 4H, $CH_2CH_2CH_3$), 2.35 (t, 4H, 2 a-SCH_2), 2.43 (t, 4H, 2 a-NCH_2), 2.46 (t, 4H, 2 e-SCH_2), 2.69 (t, 4H, 2 e-NCH_2) ppm. $^{13}C\{^1H\}$ NMR (125.7 MHz, $CDCl_3$): 11.68 ($CH_2CH_2CH_3$), 20.36 ($CH_2CH_2CH_3$), 23.65 (a-SCH_2), 38.13 (e-SCH_2), 55.08 (a-NCH_2), 56.02 (e-NCH_2), 57.03 ($CH_2CH_2CH_3$), 208.87 (CO) ppm. ESI-MS: *m*/*z* 914.8 {**1a** + $H^+\}^+$. Anal. Calcd for $C_{26}H_{30}Fe_4N_2O_{12}S_4$: C, 34.16; H, 3.31; N, 3.06; S, 14.03. Found: C, 34.16; H, 3.34; N, 3.00; S, 14.05.

Synthesis of [$Fe_2(\mu\text{-}S(CH_2)_2N^{i}Pr(CH_2)_2S)(CO)_6]_2$, 1b. Complex **1b** was prepared according to the procedure for **1a** with the appropriate dithiolate ligand, $^iPrN(CH_2CH_2SH)_2$. The yield was 17%. Red crystals were grown from hexane at −20 °C. IR (hexane, cm^{-1}): ν_{CO} 2069 (m), 2036 (vs), 1999 (s), 1987 (s), 1973 (w), 1955 (vw). ^1H NMR (500 MHz, $CDCl_3$): 1.01 (d, $^3J_{HH}$ = 6.5 Hz, 12H, $NCH(CH_3)_2$), 2.38 (s, 8H, 2 a-SCH_2, 2 e-NCH_2), 2.44 (t, 4H, 2 e-SCH_2), 2.69 (sep, 2H, 2 NCH), 2.74 (t, 4H, 2 e-NCH_2) ppm. $^{13}C\{^1H\}$ NMR (125.7 MHz, $CDCl_3$): 17.78 ($NCH(CH_3)_2$), 24.57 (a-SCH_2), 38.68 (e-SCH_2), 49.62 (a-NCH_2), 49.98 (NCH), 53.57 (e-NCH_2), 208.96 (CO) ppm. ESI-MS: *m*/*z* 914.8 {**1b** + $H^+\}^+$. Anal. Calcd for $C_{26}H_{30}Fe_4N_2O_{12}S_4$: C, 34.16; H, 3.31; N, 3.06. Found: C, 34.39; H, 3.59; N, 2.90.

Synthesis of [$Fe_2(\mu\text{-}S(CH_2)_2N^{n}Pr(CH_2)_2S)(CO)_5(PPh_3)]_2$, 2. A Schlenk flask was charged with **1a** (215 mg, 0.5 mmol) and PPh_3 (384 mg, 1 mmol) in toluene (40 mL). The solution was refluxed for 1 h, and the solvent was then removed under reduced pressure after cooled to room temperature. The crude product was purified by chromatography on silica gel, eluting first with CH_2Cl_2/hexane (v/v 1/4) to remove any unreacted starting materials, then with CH_2Cl_2 to elute the product. [$Fe_2(\mu\text{-}S(CH_2)_2N^{n}Pr(CH_2)_2S)(CO)_5(PPh_3)]_2$, **2**, was obtained as a red solid in 75% yield (379 mg) after removal of solvent. Deep-red crystals of **2** were grown from the CH_2Cl_2/hexane solution at −20 °C. IR (CH_2Cl_2, cm^{-1}): ν_{CO} 2042 (s), 1979 (vs), 1957 (sh), 1924 (w). ^1H NMR (500 MHz, CD_2Cl_2): 0.71 (t,

---

(37) (a) Harley-Mason, J. *J. Chem. Soc.* **1947**, 320–322. (b) Karlin, K. D.; Lippard, S. J. *J. Am. Chem. Soc.* **1976**, *98*, 6951–6957. (c) Snyder, H. R.; Stewart, J. M.; Ziegler, J. B. *J. Am. Chem. Soc.* **1947**, *69*, 2672–2674.

(38) *SHELXTL*, version 6.10; Bruker Analytical X-Ray Systems: Madison, WI, 2000.

$^3J_{\mathrm{HH}}$ = 7.5 Hz, 6H, 2 $\mathrm{CH_2CH_2C}H_3$), 0.93 (m, 2H, $\mathrm{CH_2C}H_2\mathrm{CH_3}$), 1.05 (m, 4H, $\mathrm{CH_2C}H_2\mathrm{CH_3}$, e-$\mathrm{SC}H_2$), 1.31 (m, 2H, a-$\mathrm{SC}H_2$), 1.86 (m, 2H, $CH_2\mathrm{CH_2CH_3}$), 1.95 (m, 2H, $CH_2\mathrm{CH_2CH_3}$), 2.05 (m, 2H, e-$\mathrm{SC}H_2$), 2.15 (m, 6H, a-$\mathrm{SC}H_2$, 2 a-$\mathrm{NC}H_2$), 2.21 (m, 2H, e-$\mathrm{NC}H_2$), 2.45 (m, 2H, e-$\mathrm{NC}H_2$), 7.44 (m, 18H, 6 *m*-, *p*-$\mathrm{C_6}H_5$), 7.58 (m, 12H, 6 *o*-$\mathrm{C_6}H_5$) ppm. $^{13}\mathrm{C}\{^1\mathrm{H}\}$ NMR (125.7 MHz, $\mathrm{CD_2Cl_2}$): 11.25 ($\mathrm{CH_2CH_2}C\mathrm{H_3}$), 19.51 ($\mathrm{CH_2}C\mathrm{H_2CH_3}$), 24.16 (a-$\mathrm{S}C\mathrm{H_2}$), 37.45 (e-$\mathrm{S}C\mathrm{H_2}$), 55.01 ($C\mathrm{H_2CH_2CH_3}$), 57.72 (e-$\mathrm{N}C\mathrm{H_2}$), 58.09 (a-$\mathrm{N}C\mathrm{H_2}$), 128.27, 128.34, 129.88, 129.96, 133.03, 133.12, 135.88, 136.19 ($\mathrm{P(}C_6\mathrm{H_5)_3}$), 210.98 ($C\mathrm{O}$) ppm. $^{31}\mathrm{P}\{^1\mathrm{H}\}$ NMR (202.48 MHz, $\mathrm{CD_2Cl_2}$): 61.06 ppm. ESI-MS: *m*/*z* 1382.9 $\{\mathbf{2} + \mathrm{H}^+\}^+$, 1355.0 $\{\mathbf{2} - \mathrm{CO} + \mathrm{H}^+\}^+$, 1327.0 $\{\mathbf{2} - 2\mathrm{CO} + \mathrm{H}^+\}^+$, 1148.9 $\{\mathbf{2} - \mathrm{PPh_3} + \mathrm{CO} + \mathrm{H}^+\}^+$. Anal. Calcd for $\mathrm{C_{60}H_{60}Fe_4N_2O_{10}S_4P_2}$: C, 52.12; H, 4.37; N, 2.03; S, 9.28. Found: C, 51.66; H, 4.34; N, 2.00; S, 9.29.

Synthesis of $[\mathrm{Fe_2}(\mu\text{-}\mathrm{S(CH_2)_2N}^n\mathrm{Pr(Me)(CH_2)_2S)(CO)_6}]_2^{2+}$, $[\mathbf{1a\text{-}2Me}^{\mathrm{N}}]^{2+}$. To a solution of **1a** (400 mg, 0.44 mmol) in $\mathrm{CH_2Cl_2}$ (20 mL) was added excess MeOTf (600 μL, 5.48 mmol). The solution was stirred for 1 h and some orange precipitate appeared. The stirring was continued for additional 6 h before the solvent volume was decreased to 3 mL. Addition of 20 mL diethyl ether led to precipitation of the orange-red solid. It was washed three times with $\mathrm{CH_2Cl_2}$/ether and dried in vacuo. The *N*-methylated product $[\mathrm{Fe_2}(\mu\text{-}\mathrm{S(CH_2)_2N}^n\mathrm{Pr(Me)(CH_2)_2S)(CO)_6}]_2\mathrm{(OTf)_2}$, $[\mathbf{1a\text{-}2Me}^{\mathrm{N}}]\mathrm{(OTf)_2}$, was obtained in 77% yield (419 mg). Orange-red crystals of $[\mathbf{1a\text{-}2Me}^{\mathrm{N}}]\mathrm{(OTf)_2 \cdot 4CH_2Cl_2}$ were grown from the $\mathrm{CH_2Cl_2}$/ether solution at −20 °C. IR ($\mathrm{CH_3CN}$, $\mathrm{cm^{-1}}$): ν_{CO} 2080 (m), 2049 (vs), 2007 (s), 1985 (sh). IR ($\mathrm{CH_2Cl_2}$, $\mathrm{cm^{-1}}$): ν_{CO} 2081 (m), 2051 (vs), 2008 (s), 1986 (m). ^{1}H NMR (500 MHz, $\mathrm{CD_3C(O)CD_3}$): 0.91 (t, 6H, 2 $\mathrm{CH_2CH_2C}H_3$), 1.89 (m, 4H, 2 $\mathrm{CH_2C}H_2\mathrm{CH_3}$), 2.60−2.92 (m, 8H, 8 $\mathrm{SC}H_2$), 3.26 (s, 3H, $\mathrm{NC}H_3$), 3.27 (s, 3H, $\mathrm{NC}H_3$), 3.35−4.13 (m, 12H, 6 $\mathrm{NC}H_2$) ppm. ESI-MS: *m*/*z* 1092.7 $\{[\mathbf{1a\text{-}2Me}^{\mathrm{N}}]\mathrm{(OTf)}\}^+$, 1008.8 $\{[\mathbf{1a\text{-}2Me}^{\mathrm{N}}]\mathrm{(OTf)} - 3\mathrm{CO}\}^+$, 980.8 $\{[\mathbf{1a\text{-}2Me}^{\mathrm{N}}]\mathrm{(OTf)} - 4\mathrm{CO}\}^+$, 952.8 $\{[\mathbf{1a\text{-}2Me}^{\mathrm{N}}]\mathrm{(OTf)} - 5\mathrm{CO}\}^+$, 924.8 $\{[\mathbf{1a\text{-}2Me}^{\mathrm{N}}]\mathrm{(OTf)} - 6\mathrm{CO}\}^+$, 471.9 $\{[\mathbf{1a\text{-}2Me}^{\mathrm{N}}]\}^{2+}$. Anal. Calcd for $\mathrm{C_{34}H_{44}Cl_8F_6Fe_4N_2O_{18}S_6}$: C, 29.00; H, 2.92; N, 2.25. Found: C, 29.11; H, 3.02; N, 2.25.

Synthesis of $[\mathrm{Fe_2}(\mu\text{-}\mathrm{S(CH_2)_2N}^n\mathrm{Pr(H)(CH_2)_2S)(CO)_6}]_2^{2+}$, $[\mathbf{1a\text{-}2H}^{\mathrm{N}}]^{2+}$. To a solution of **1a** (200 mg, 0.22 mmol) in $\mathrm{CH_2Cl_2}$ (8 mL) was added excess $\mathrm{HBF_4}$ (139 μL, 1.1 mmol). The solution was stirred for 10 min and turned to orange accompanying the appearance of an orange solid. The solvent volume was reduced to 3 mL, and then addition of 25 mL diethyl ether led to more precipitation of the orange solid. It was washed three times with ether and dried in vacuo. The *N*-protonated product $[\mathbf{1a\text{-}2H}^{\mathrm{N}}]\mathrm{(BF_4)_2}$, $[\mathrm{Fe_2}(\mu\text{-}\mathrm{S(CH_2)_2N}^n\mathrm{Pr(H)(CH_2)_2S)(CO)_6}]_2\mathrm{(BF_4)_2}$, was obtained in 95% (227 mg) yield. Orange-red crystals of $[\mathbf{1a\text{-}2H}^{\mathrm{N}}]\mathrm{(BF_4)_2 \cdot 2CH_3C(O)CH_3}$ were grown from the acetone/hexane solution at −20 °C. IR ($\mathrm{CH_2Cl_2}$, $\mathrm{cm^{-1}}$): ν_{CO} 2079 (m), 2048 (s), 2004 (s). IR ($\mathrm{CH_3CN}$, $\mathrm{cm^{-1}}$): ν_{CO} 2080 (m), 2048 (s), 2004 (s). ^{1}H NMR (500 MHz, $\mathrm{CD_3CN}$): 0.95 (t, $^3J_{\mathrm{HH}}$ = 7 Hz, 6H, $\mathrm{CH_2CH_2C}H_3$), 1.70 (m, 2H, $\mathrm{CH_2C}H_2\mathrm{CH_3}$), 1.77 (m, 2H, $\mathrm{CH_2C}H_2\mathrm{CH_3}$), 2.48 (m, 2H, a-$\mathrm{SC}H_2$), 2.56 (m, 2H, a-$\mathrm{SC}H_2$), 2.65 (m, 2H, e-$\mathrm{SC}H_2$), 2.70 (m, 2H, e-$\mathrm{SC}H_2$), 3.10 (m, 4H, 2 a-$\mathrm{NC}H_2$), 3.16 (m, 4H, 2 $\mathrm{C}H_2\mathrm{CH_2CH_3}$), 3.39 (m, 2H, e-$\mathrm{NC}H_2$), 3.45 (m, 2H, e-$\mathrm{NC}H_2$), 6.96, 7.06 (br, 2H, 2 $\mathrm{N}H$, *syn*, *anti*) ppm. $^{13}\mathrm{C}\{^1\mathrm{H}\}$ NMR (125.7 MHz, $\mathrm{CD_3CN}$): 10.93 ($\mathrm{CH_2CH_2}C\mathrm{H_3}$), 17.92 ($\mathrm{CH_2}C\mathrm{H_2CH_3}$), 18.95 (a-$\mathrm{S}C\mathrm{H_2}$), 32.75 (e-$\mathrm{S}C\mathrm{H_2}$), 54.04 (a-$\mathrm{N}C\mathrm{H_2}$), 55.29 (e-$\mathrm{N}C\mathrm{H_2}$), 58.91 ($C\mathrm{H_2CH_2CH_3}$), 209.04 ($C\mathrm{O}$) ppm. ESI-MS: *m*/*z* 1002.8 $\{[\mathbf{1a{-}2H}^{\mathrm{N}}]\mathrm{(BF_4)}\}^+$. Anal. Calcd for $\mathrm{C_{26}H_{32}B_2F_8Fe_4N_2O_{12}S_4}$: C, 28.65; H, 2.96; N, 2.57; S, 11.77. Found: C, 28.73; H, 3.03; N, 2.50; S, 11.67.

Reaction of $[\mathrm{Fe_2}(\mu\text{-}\mathrm{S(CH_2)_2N}^n\mathrm{Pr(CH_2)_2S)(CO)_6}]_2$ with Various Acids ($\mathrm{HClO_4}$, HOTf). The procedure is the same as described for $\mathrm{HBF_4}$. All $[\mathbf{1a\text{-}2H}^{\mathrm{N}}]^{2+}$ salts with appropriate anions were obtained in the yield of greater than 90%. $[\mathbf{1a{-}2H}^{\mathrm{N}}]\mathrm{(OTf)_2}$: IR ($\mathrm{CH_3CN}$, $\mathrm{cm^{-1}}$): ν_{CO} 2079 (m), 2047 (s), 2005 (s). $[\mathbf{1a\text{-}2H}^{\mathrm{N}}]\mathrm{(ClO_4)_2}$: IR ($\mathrm{CH_3CN}$, $\mathrm{cm^{-1}}$): ν_{CO} 2078 (m), 2046 (s), 2002 (s).

Synthesis of $[\mathrm{Fe_2}(\mu\text{-}\mathrm{S(CH_2)_2N}^n\mathrm{Pr(H)(CH_2)_2S)(CO)_5(PPh_3)}]_2^{2+}$, $[\mathbf{2{-}2H}^{\mathrm{N}}]^{2+}$. To a solution of **2** (302 mg, 0.22 mmol) in $\mathrm{CH_2Cl_2}$ (15 mL) was added excess $\mathrm{HBF_4}$ (165 μL, 1.31 mmol). A suspension of **2** slowly went into the reaction solution, and the solution was stirred for 2 h. The solvent volume was reduced to 3 mL, and then addition of 25 mL diethyl ether led to precipitation of the deep-red solid. It was washed three times with ether and dried in vacuo. The *N*-protonated product $[\mathbf{2{-}2H}^{\mathrm{N}}]\mathrm{(BF_4)_2}$, $[\mathrm{Fe_2}(\mu\text{-}\mathrm{S(CH_2)_2N}^n\mathrm{Pr(H)(CH_2)_2S)(CO)_5(PPh_3)}]_2\mathrm{(BF_4)_2}$, was obtained in 89% yield (305 mg). Deep-red crystals of $[\mathbf{2{-}2H}^{\mathrm{N}}]\mathrm{(BF_4)_2 \cdot 2CH_2Cl_2}$ were grown from the $\mathrm{CH_2Cl_2}$/ether solution at −20 °C. IR ($\mathrm{CH_2Cl_2}$, $\mathrm{cm^{-1}}$): ν_{CO} 2053 (s), 1992 (vs), 1966 (m), 1944 (w), 1926 (sh). IR ($\mathrm{CH_3CN}$, $\mathrm{cm^{-1}}$): ν_{CO} 2052 (s), 1990 (vs), 1970 (sh), 1939 (w), 1927 (sh). ^{1}H NMR (500 MHz, $\mathrm{CD_2Cl_2}$): 0.86−0.95 (m, 6H, 2 $\mathrm{CH_2CH_2C}H_3$), 1.36−1.47 (m, 4H, 2 $\mathrm{CH_2C}H_2\mathrm{CH_3}$), 1.93−3.24 (m, 20H, 2 $\mathrm{C}H_2\mathrm{CH_2CH_3}$, 4 $\mathrm{NC}H_2$, 4 $\mathrm{SC}H_2$), 7.18−7.66 (m, 30H, 6 $\mathrm{C_6}H_5$), 7.37, 7.72, 7.91 (br, 2H, 2 $\mathrm{N}H$, *syn*, *anti*) ppm. $^{13}\mathrm{C}\{^1\mathrm{H}\}$ NMR (125.7 MHz, $\mathrm{CD_2Cl_2}$, 253 K): 10.51 ($\mathrm{CH_2CH_2}C\mathrm{H_3}$), 10.58 ($\mathrm{CH_2CH_2}C\mathrm{H_3}$), 14.13 ($\mathrm{S}C\mathrm{H_2}$), 17.18 (2 $\mathrm{CH_2}C\mathrm{H_2CH_3}$), 17.91 (2 $\mathrm{S}C\mathrm{H_2}$), 29.84 ($\mathrm{N}C\mathrm{H_2}$), 30.23 ($\mathrm{S}C\mathrm{H_2}$), 54.43 ($\mathrm{N}C\mathrm{H_2}$), 55.96 ($\mathrm{N}C\mathrm{H_2}$), 56.29 (2 $C\mathrm{H_2CH_2CH_3}$), 56.62 ($\mathrm{N}C\mathrm{H_2}$), 128.81, 128.89, 129.05, 130.86, 133.21, 133.29 ($\mathrm{P(}C_6\mathrm{H_5)_3}$), 209.03, 214.99 ($C\mathrm{O}$) ppm. $^{31}\mathrm{P}\{^1\mathrm{H}\}$ NMR (202.48 MHz, $\mathrm{CD_2Cl_2}$): 57.65 (*syn*), 59.37 (*anti*), 64.38 (*syn*) ppm. ESI-MS: *m*/*z* 1471.0 $\{[\mathbf{2{-}2H}^{\mathrm{N}}]\mathrm{(BF_4)}\}^+$, 1382.9 $\{[\mathbf{2{-}2H}^{\mathrm{N}}] - \mathrm{H}^+\}^+$, 1148.9 $\{[\mathbf{2{-}2H}^{\mathrm{N}}] + \mathrm{CO} - \mathrm{PPh_3} - \mathrm{H}^+\}^+$, 692.0 $\{[\mathbf{2{-}2H}^{\mathrm{N}}]\}^{2+}$. Anal. Calcd for $\mathrm{C_{60}H_{62}B_2F_8Fe_4N_2O_{10}S_4P_2}$: C, 46.24; H, 4.01; N, 1.80. Found: C, 45.96; H, 4.10; N, 1.80.

Reaction of $[\mathbf{1a\text{-}2H}^{\mathrm{N}}]^{2+}$ with $\mathrm{PPh_3}$. $[\mathbf{2{-}2H}^{\mathrm{N}}]^{2+}$ can also be synthesized from $[\mathbf{1a\text{-}2H}^{\mathrm{N}}]^{2+}$. A Schlenk flask was charged with $[\mathbf{1a\text{-}2H}^{\mathrm{N}}]^{2+}$ (545 mg, 0.5 mmol) and $\mathrm{PPh_3}$ (960 mg, 2.5 mmol) in $\mathrm{CH_2Cl_2}$ (30 mL). The solution was stirred at room temperature overnight. When the reaction was completed, monitored by IR, the solution was removed under reduced pressure. The solid was washed by $\mathrm{CH_2Cl_2}$/ether three times and dried under vacuum. $[\mathbf{2{-}2H}^{\mathrm{N}}]^{2+}$ was obtained as a red solid in 60% yield (467 mg). $[\mathbf{2{-}2H}^{\mathrm{N}}]\mathrm{(BF_4)_2}$: IR ($\mathrm{CH_2Cl_2}$, $\mathrm{cm^{-1}}$): ν_{CO} 2053 (s), 1992 (vs), 1966 (m), 1944 (w), 1926 (sh).

Synthesis of $[\mathrm{Fe_2}(\mu\text{-}\mathrm{S(CH_2)_2N}^n\mathrm{Pr(CH_2)_2S)(CO)_5(P}^n\mathrm{Bu_3)}]_2$, 3. To a Schlenk flask containing **1a** (400 mg, 0.44 mmol) in 14 mL of toluene was added neat $\mathrm{P}^n\mathrm{Bu_3}$ (0.24 mL, 0.96 mmol) by microsyringe. The solution was heated to 90 °C for at least 0.5 h under $\mathrm{N_2}$ and monitored by IR spectroscopy to ensure that the reaction was completed. The red brown solution was dried under reduced pressure after being cooled to RT. Several portions of $\mathrm{CH_2Cl_2}$/MeOH were used to wash the solid, and it was then dried under vacuum to afford the red brown solid. The complex **3**, $[\mathrm{Fe_2}(\mu\text{-}\mathrm{S(CH_2)_2N}^n\mathrm{Pr(CH_2)_2S)(CO)_5(P}^n\mathrm{Bu_3)}]_2$, was obtained in 63% yield (348 mg). Red crystals of **3** were grown from the $\mathrm{CH_2Cl_2}$ solution layered with MeOH at −20 °C. IR ($\mathrm{CH_2Cl_2}$, $\mathrm{cm^{-1}}$): ν_{CO} 2037 (s), 1975 (vs), 1961 (s), 1916 (w). ^{1}H NMR (500 MHz, $\mathrm{CD_2Cl_2}$, 253 K): 0.81 (t, $^3J_{\mathrm{HH}}$ = 7.5 Hz, 6H, 2 $\mathrm{NCH_2CH_2C}H_3$), 0.94 (t, $^3J_{\mathrm{HH}}$ = 7.5 Hz, 18H, 2 $\mathrm{P(CH_2CH_2CH_2C}H_3\mathrm{)_3}$), 1.41 (m, 16H, 2 $\mathrm{NCH_2C}H_2\mathrm{CH_3}$, 2 $\mathrm{P(CH_2CH_2C}H_2\mathrm{CH_3)_3}$), 1.49 (m, 12H, 2 $\mathrm{P(CH_2C}H_2\mathrm{CH_2CH_3)_3}$), 1.72 (m, 6H, $\mathrm{P(C}H_2\mathrm{CH_2CH_2CH_3)_3}$), 1.80 (m, 6H, $\mathrm{P(C}H_2\mathrm{CH_2CH_2CH_3)_3}$), 2.30 (m, 8H, 4 $\mathrm{C}H_2$), 2.40−2.50 (m, 8H, 4 $\mathrm{C}H_2$), 2.65 (m, 4H, 2 $\mathrm{C}H_2$) ppm. $^{13}\mathrm{C}\{^1\mathrm{H}\}$ NMR (125.7 MHz, $\mathrm{CD_2Cl_2}$, 253 K): 12.08 ($\mathrm{NCH_2CH_2}C\mathrm{H_3}$), 14.22 ($\mathrm{P(CH_2CH_2CH_2}C\mathrm{H_3)_3}$), 20.51 ($\mathrm{NCH_2}C\mathrm{H_2CH_3}$), 24.82, 24.92 ($\mathrm{P(CH_2CH_2}C\mathrm{H_2CH_3)_3}$), 26.05 ($\mathrm{P(CH_2}C\mathrm{H_2CH_2CH_3)_3}$), 28.75 ($\mathrm{P(}C\mathrm{H_2CH_2CH_2CH_3)_3}$), 36.76 ($C\mathrm{H_2}$), 55.89 ($C\mathrm{H_2}$), 57.14 ($C\mathrm{H_2}$), 212.20, 215.66, 216.73 ($C\mathrm{O}$) ppm. $^{31}\mathrm{P}\{^1\mathrm{H}\}$ NMR (202.48 MHz, $\mathrm{CD_2Cl_2}$): 43.62 ppm. ESI-MS: *m*/*z* 1263.2 $\{\mathbf{3} + \mathrm{H}^+\}^+$. Anal. Calcd for $\mathrm{C_{48}H_{84}Fe_4N_2O_{10}P_2S_4}$: C, 45.65; H, 6.70; N, 2.22. Found: C, 45.55; H, 6.71; N, 2.20.

Synthesis of $[\mathrm{Fe_2}(\mu\text{-}\mathrm{S(CH_2)_5S)(CO)_6}]_2$, 4. To a solution of $\mathrm{Fe_3(CO)_{12}}$ (2 g, 3.97 mmol) in 36 mL of $\mathrm{CH_2Cl_2}$ was added $\mathrm{HS(CH_2)_5SH}$ (540 μL, 4.03 mmol). Solvent was removed in vacuum to obtain a dark red-colored residue after refluxing 30 min. The crude product was purified by chromatography on silica gel with hexane as the eluent. The yellow orange band was collected and dried to give an orange powder of $[Fe_2(\mu\text{-}S(CH_2)_5S)(CO)_6]_2$, **4**, in 5.3% (88 mg) yield. Orange-red crystals of **4** were grown from the saturated solution in hexane at −20 °C. IR (hexane, cm^{-1}): ν_{CO} 2071 (m), 2038 (vs), 2001 (s), 1993 (s), 1975 (w), 1958 (vw). IR (CH_2Cl_2, cm^{-1}): ν_{CO} 2070 (m), 2036 (vs), 1992 (s). ^{1}H NMR (500 MHz, $CDCl_3$): 1.33 (m, 6H, 2 $CH_2\mathit{CH}_2(CH_2)_3$, $S\mathit{CH}_2$), 1.78 (m, 4H, 2 $CH_2\mathit{CH}_2(CH_2)_3$), 2.04 (m, 6H, 2 $(CH_2)_2\mathit{CH}_2(CH_2)_2$, $S\mathit{CH}_2$), 2.54 (t, 4H, 2 $S\mathit{CH}_2$) ppm. $^{13}C\{^1H\}$ NMR (125.7 MHz, $CDCl_3$): 23.35 (2 $(CH_2)_2\mathit{C}H_2(CH_2)_2$), 24.57 ($S\mathit{C}H_2$), 28.53 ($S\mathit{C}H_2$), 30.59 (2 $CH_2\mathit{C}H_2(CH_2)_3$), 31.19 (2 $CH_2\mathit{C}H_2(CH_2)_3$), 38.59 (2 $S\mathit{C}H_2$), 208.67 ($\mathit{C}O$) ppm. EI+-MS: *m*/*z* 827.5 $\{\mathbf{4}\}^+$, 799.5 $\{\mathbf{4} - CO\}^+$, 743.5 $\{\mathbf{4} - 3CO\}^+$, 715.5 $\{\mathbf{4} - 4CO\}^+$, 687.5 $\{\mathbf{4} - 5CO\}^+$, 659.6 $\{\mathbf{4} - 6CO\}^+$, 603.6 $\{\mathbf{4} - 8CO\}^+$, 575.6 $\{\mathbf{4} - 9CO\}^+$, 547.6 $\{\mathbf{4} - 10CO\}^+$, 519.6 $\{\mathbf{4} - 11CO\}^+$, 491.6 $\{\mathbf{4} - 12CO\}^+$. Anal. Calcd for $C_{22}H_{20}Fe_4O_{12}S_4$: C, 31.91; H, 2.43; S, 15.46. Found: C, 32.30; H, 2.48; S, 15.32.

Acknowledgment. We are grateful to financial support from National Science Council of Taiwan and Academia Sinica. We thank Prof. Wen-Feng Liaw (National Tsing Hua University) and Prof. Marcetta Y. Darensbourg (Texas A&M University) for insightful discussions. We also thank Drs. Mei-Chun Tseng and Su-Ching Lin for help with MS analysis and 2D NMR experiments, respectively.

Supporting Information Available: Crystallographic data in CIF format and crystallographic table (Table *S1*) for **1a**, $\mathbf{1a_{asym}}$, **1b**, $[\mathbf{1a\text{-}2Me^N}]^{2+}$, $[\mathbf{1a\text{-}2H^N}]^{2+}$, **2**, $[\mathbf{2{-}2H^N}]^{2+}$, **3**, and **4**. Molecular structure of $\mathbf{1a_{asym}}$ (Figure *S1*). The table of the benchmark model complexes (Table *S2*). The IR (Figures *S2*, *S9c*, *S14*), UV−vis (Figure *S13*) spectra, and cyclic voltammograms (Figures *S3-S8*, *S9a*, *S9b*, *S10-S12*). This material is available free of charge via the Internet at http://pubs.acs.org.